Bull Volcanol (2015) 77: 45
DOI 10.1007/s00445-015-0932-0

RESEARCH ARTICLE

$^{40}Ar/^{39}Ar$ geochronology and geochemistry of the Central Saurashtra mafic dyke swarm: insights into magmatic evolution, magma transport, and dyke-flow relationships in the northwestern Deccan Traps

Ciro Cucciniello[1] · **Elena I. Demonterova**[2] · **Hetu Sheth**[3] · **Kanchan Pande**[3] · **Anjali Vijayan**[3]

Received: 21 November 2014 / Accepted: 11 April 2015 / Published online: 5 May 2015

Abstract The Central Saurashtra mafic dyke swarm in the northwestern Deccan Traps contains a few picrites, several subalkalic basalts and basaltic andesites, and an andesite. We have obtained precise $^{40}Ar/^{39}Ar$ ages of 65.6±0.2 Ma, 66.6±0.3, and 62.4±0.3 Ma (2σ errors) for three of the dykes, indicating the emplacement of the swarm over several million years. Mineral chemical and whole-rock major and trace element and Sr–Nd isotopic data show that fractional crystallization and crystal accumulation were important processes. Except for two dykes (with $\varepsilon_{Nd}t$ values of –8.2 and –12.3), the magmas were only moderately contaminated by continental crust. The late-emplaced (62.4 Ma) basalt dyke has compositional characteristics (low La/Sm and Th/Nb, high $\varepsilon_{Nd}t$ of +4.3) suggesting little or no crustal contamination. Most dykes are low-Ti and a few high-Ti, and these contrasting Ti types cannot be produced by fractional crystallization processes but require distinct parental magmas. Some dykes are compositionally homogeneous over tens of kilometers, whereas others are heterogeneous, partly because they were formed by multiple magma injections. The combined field and geochemical data establish the Sardhar dyke as ≥62 km long and the longest in Saurashtra, but this and the other Central Saurasthra dykes cannot have fed any of the hitherto studied lava-flow sequences in Saurashtra, given their very distinct Sr–Nd isotopic compositions. As observed previously, high-Ti lavas and dykes only outcrop east–northeast of a line joining Rajkot and Palitana, probably because of underlying enriched mantle at ~65 Ma.

Keywords Volcanism · Deccan Traps · Flood basalt · Dyke swarms · India · Saurashtra

Editorial responsibility: D.W. Peate

Electronic supplementary material The online version of this article (doi:10.1007/s00445-015-0932-0) contains supplementary material, which is available to authorized users.

✉ Ciro Cucciniello
ciro.cucciniello@unina.it

[1] Dipartimento di Scienze della Terra, dell'Ambiente e delle Risorse (DiSTAR), Università di Napoli Federico II, via Mezzocannone 8, 80134 Napoli (Naples), Italy

[2] Institute of the Earth's Crust, Siberian Branch of the Russian Academy of Sciences, Irkutsk, Russia

[3] Department of Earth Sciences, Indian Institute of Technology Bombay, Powai, Mumbai 400076, India

Introduction

Recent geochemical studies of the Deccan Traps lava flows and dyke swarms (Fig. 1a) have shown that whereas many lava-flow successions, separated by hundreds of kilometers, correlate stratigraphically with each other (e.g., Peng et al. 2014), many others do not, and thus the Deccan lava eruptions were polycentric (e.g., Sheth and Melluso 2008; Sheth et al. 2013). Three major mafic dyke swarms outcropping in the Deccan province (Fig. 1a) have been studied extensively in the search for the feeder dykes of the Deccan Traps lava flows, and some of the dykes are inferred to have fed lava flows several hundred kilometers in length (e.g., Bondre et al. 2006; Ray et al. 2007; Sheth et al. 2009, 2013, 2014; Vanderkluysen et al. 2011).

The northwestern Deccan Traps (including the Saurashtra, Kachchh, and Rajasthan regions, Fig. 1a) remain poorly studied in comparison to the southwestern Deccan (Western Ghats), the central Deccan (the Dhule area), and the northern and northeastern Deccan regions. Geochronological data for the northwestern Deccan Traps are particularly scarce. Here, we present a study of the large Central Saurashtra mafic dyke swarm in the northwestern Deccan Traps. With varied datasets (field, petrographic, $^{40}Ar/^{39}Ar$ geochronological, mineral chemical, and whole-rock geochemical data, including major and trace element and Sr–Nd isotopic data), we discuss the magmatic evolution and magma transport in these dykes and examine the tectonomagmatic relationship of this dyke swarm with the lava-flow sequences in the Saurashtra region.

Geology

Saurashtra (Fig. 1a, b) is mostly flat and low-lying and covered by the Deccan flood basalts in large part. Geological, geophysical and drilling data suggest that the basalts are up to a few hundred meters thick (e.g., West 1958; Sheth et al. 2013). Mesozoic sedimentary rocks outcrop in the northern areas and Tertiary and Quaternary sediments outcrop along the coastal fringes of Saurashtra. Unlike the main Deccan province to the east–southeast, dominated by tholeiitic flood lavas, the Deccan Traps of Saurashtra include several volcano-plutonic complexes and a great range of rock types including picrite and ankaramite, lamprophyres, diorite, granophyre, and rhyolite (e.g., Melluso et al. 1995; Sheth et al. 2011, 2012; Kshirsagar et al. 2012, and references therein). Mafic dykes are abundant (Auden 1949), and the Eastern Saurashtra dykes studied by Sheth et al. (2013) represent a westerly extension of the large, ENE–WSW trending Narmada-Tapi dyke swarm (NTDS, Fig. 1a) into Saurashtra across the Cambay rift.

The Central Saurashtra dykes studied here form a large swarm exposed between the cities of Rajkot and Amreli, ~150 km northwest of the Eastern Saurashtra dyke swarm (Fig. 1b). This area is the relatively elevated (~200 m above mean sea level) but flat central highland region of Saurashtra, and the dykes form linear topographic ridges many kilometers long. They intrude basaltic lava flows at the current level of exposure and may have fed lava flows at higher levels subsequently eroded away. The Central Saurashtra dyke swarm (Fig. 1c) contains several dykes trending ENE–WSW, and others with different orientations including ~ E–W and NW–SE. We collected 19 samples of the Central Saurashtra dykes, which are all mafic and medium to very fine grained. Field notes and sample descriptions are provided in the Supplementary Table S1.

Fig. 1 Geological maps of the Deccan Traps (**a**) and of Saurashtra (**b**), with important features and localities mentioned in the text marked in both. Elliptical area in (**a**) is the northwestern Deccan region, with great compositional diversity and many igneous complexes (Sheth et al. 2011, 2012). Three major dyke swarms in the Deccan Traps are shown: the Narmada-Tapi dyke swarm (*NTDS*), the Coastal dyke swarm (*CDS*), and the Nasik-Pune swarm (*NPDS*, Vanderkluysen et al. 2011 and references therein). Also shown in panel (**b**) are drillhole lava sequences in NE Saurashtra (*black stars*) located at Wadhwan, Dhandhuka, and Botad, and igneous complexes of Saurashtra (*white stars*). In (**b**), the *rectangular area* shown by the *box* over central Saurashtra is the present study area. The *smaller box* shows the area of the Palitana lava sequence and Eastern Saurashtra dykes studied by Sheth et al. (2013). High-Ti lavas and dykes are only found to the north–northeast of the line joining Rajkot and Palitana cities (Melluso et al. 1995; Sheth et al. 2013). **c** Map of the present study area, showing the major topographic and geological features. The area is more or less flat-lying and forms the central Saurashtra highlands (~200 m above sea level). *Open circles* are towns and villages, and *double grey lines* are roads. The Central Saurashtra dykes are shown by *black lines*, and *filled circles* on the lines represent samples collected. Four high-Ti dykes (explained in Fig. 3) are indicated by "(HTi)" next to the sample numbers; all the other dykes are low-Ti. Numbers within grey ellipses are the 1:50,000 scale Survey of India toposheet numbers

Analytical methods

Small fresh chips of these samples were cleaned in an ultrasonic bath and ground to powders of <75 μm grain size using a Retsch PM-100 planetary ball mill and stainless steel grinding balls, in the Department of Earth Sciences, IIT Bombay. Major oxide compositions of the dykes by inductively coupled plasma atomic emission spectrometry (instrument: Jobin Yvon Ultima 2), and loss on ignition (LOI) values, were also determined there (Table 1), following the procedure described by Sheth et al. (2013). Trace elements including the rare earth elements (REE) were analyzed in 12 selected dyke samples by inductively coupled plasma mass spectrometry at the Institute of the Earth's Crust, of the Siberian Branch of the Russian Academy of Sciences, Irkutsk (Table 2). 50 mg of sample powders were weighed in 40 ml PFA vials. Dissolution was done using open vials by a mixture of HF, HNO_3, and $HClO_4$ following Panteeva et al. (2003). The measurements were performed using an Agilent 7500ce (Agilent Technologies Inc., USA) mass spectrometer operated at the Limnological Institute of the Siberian Branch of the Russian Academy of Sciences, Irkutsk. 10 ppb of In and Bi were added as internal standards to correct for instrumental drift and matrix effects. The measured mass spectra were analyzed and elemental concentrations in the samples calculated offline using Excel software and data for certified reference materials MGR-N, JB-2, and BCR-2.

Strontium and neodymium isotopic ratios were also measured in these 12 samples at the Institute of the Earth's Crust, Irkutsk (Table 3). The procedures followed Pin and Santos-Zalduegui (1997) for Nd and Pin et al. (1994) for Sr, with minor modifications outlined by Rasskazov et al. (2002)

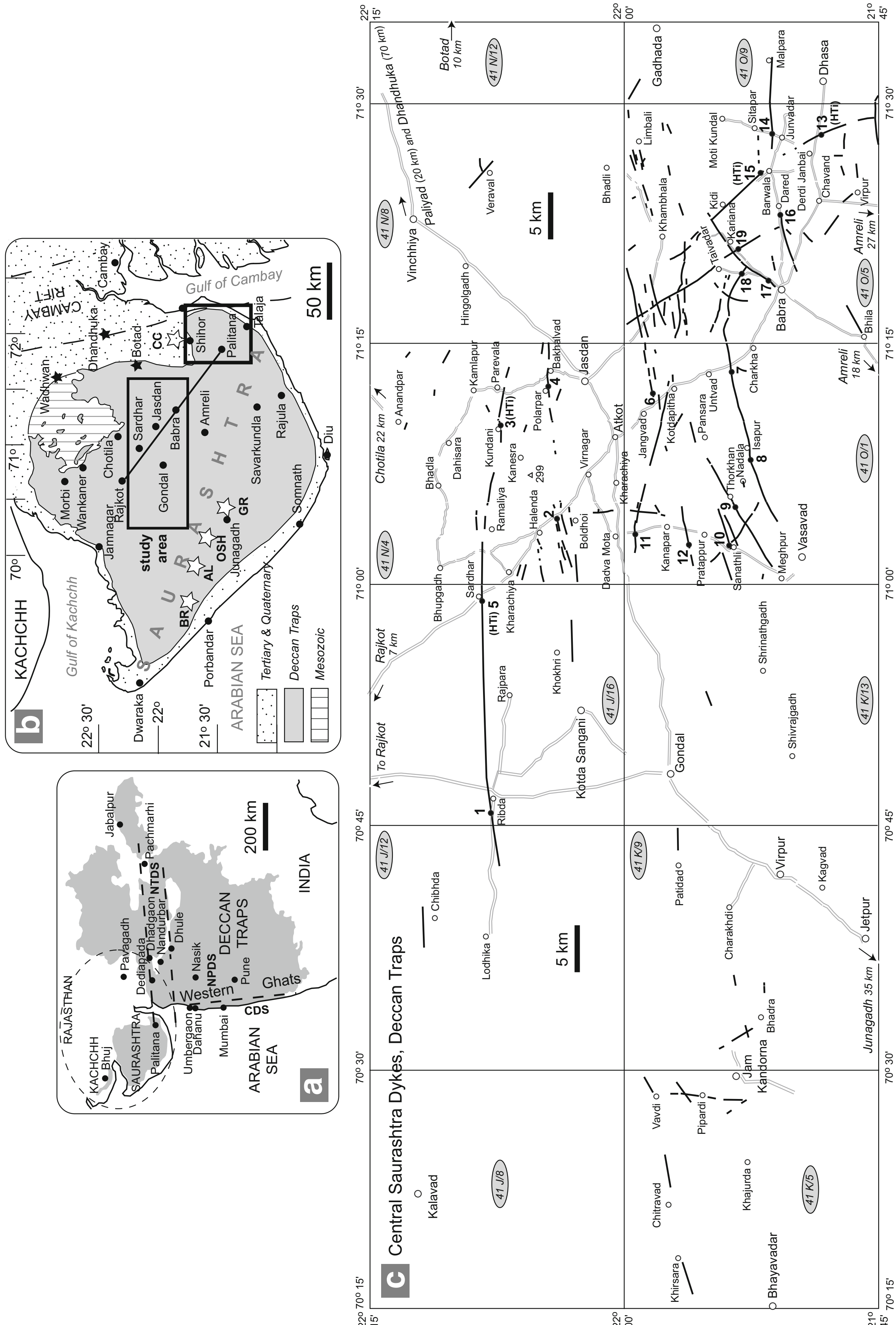
a
KACHCHH
SAURASHTRA
RAJASTHAN
ARABIAN SEA
DECCAN TRAPS
INDIA
Western Ghats
200 km
b
KACHCHH
Gulf of Kachchh
Gulf of Cambay
CAMBAY RIFT
SAURASHTRA
study area
ARABIAN SEA
50 km
Tertiary & Quaternary
Deccan Traps
Mesozoic
c
Central Saurashtra Dykes, Deccan Traps
5 km

Table 1 Major element data (in wt.%) for the Central Saurashtra dyke swarm, northwestern Deccan Traps

Trend	N80 (87)	N80	N80 (100)	N83	N90 (87)	N80	Curved (~N77)	N90 (77)	N68	N70	N80 (113)
Rock name	B, sa	B, sa	BA	B, sa	BA	BA	B, sa	PIC	PIC	B, sa	B, sa
Sample	CSD1	CSD2	CSD3	CSD4	CSD5	CSD6	CSD7	CSD8	CSD9	CSD10	CSD11
SiO_2	50.10	49.77	54.63	49.29	52.91	54.85	49.15	48.52	49.89	51.72	51.26
TiO_2	1.29	0.80	3.24	0.74	2.98	1.53	1.15	1.10	0.92	0.84	0.88
Al_2O_3	13.50	14.50	13.80	14.66	12.83	9.70	10.75	10.48	10.27	10.41	9.59
Fe_2O_3T	12.09	12.65	13.36	12.04	12.92	12.02	12.50	12.27	12.78	12.85	14.39
MnO	0.18	0.21	0.19	0.19	0.19	0.16	0.20	0.19	0.20	0.21	0.23
MgO	9.20	8.58	4.44	8.84	4.75	7.18	10.87	12.78	12.42	8.37	8.53
CaO	10.76	13.15	7.28	13.21	7.08	10.37	12.83	12.09	12.51	12.18	12.59
Na_2O	1.67	1.49	2.55	1.45	2.33	1.88	1.74	1.94	1.76	1.88	1.63
K_2O	0.39	0.13	1.93	0.15	1.79	1.21	0.55	0.60	0.31	0.34	0.44
P_2O_5	0.13	0.08	0.46	0.10	0.43	0.16	0.15	0.15	0.07	0.09	0.09
LOI	1.42	1.14	1.34	1.02	1.15	1.44	0.84	0.68	0.42	1.22	0.71
Total	100.73	102.50	103.22	101.69	99.36	100.50	100.73	100.80	101.55	100.11	100.34
Mg#	64.0	61.3	45.5	63.2	48.0	60.0	67.0	70.9	69.4	62.1	59.9

Trend	N75	Curved (~N337)	N90	N320	N80 (70)	Curved (~N48)	Curved (~N290)	N326		
Rock name	PIC	A	B, sa	BA	B, sa	B, sa	B, sa	B, sa	Meas.	Ref.
Sample	CSD12	CSD13	CSD14	CSD15	CSD16	CSD17	CSD18	CSD19	BHVO2	BHVO2
SiO_2	47.22	56.67	48.89	54.71	48.86	47.99	48.02	49.18	49.56	49.9
TiO_2	0.83	2.84	1.06	2.79	0.90	1.17	1.04	1.23	2.76	2.73
Al_2O_3	13.24	8.74	14.28	12.46	14.33	11.33	10.31	14.09	13.55	13.5
Fe_2O_3T	11.93	15.59	11.21	15.04	12.20	11.49	11.95	11.24	12.14	12.3
MnO	0.19	0.24	0.17	0.23	0.20	0.18	0.18	0.18	0.17	0.166
MgO	15.56	2.86	7.97	2.92	9.80	9.05	11.15	8.32	7.63	7.23
CaO	10.92	6.15	10.47	5.93	13.09	12.38	12.16	11.89	11.20	11.4
Na_2O	1.37	2.65	1.88	2.59	1.52	2.05	1.59	1.68	1.86	2.22
K_2O	0.45	1.78	0.69	1.67	0.34	0.65	0.40	0.45	0.52	0.52
P_2O_5	0.10	0.63	0.13	0.59	0.12	0.17	0.16	0.15	0.29	0.27
LOI	0.79	1.82	2.80	1.81	1.80	1.00	2.02	0.97		
Total	102.60	99.97	99.55	100.74	103.16	97.46	98.98	99.38	99.68	100.24
Mg#	75.3	32.3	62.4	32.8	65.2	64.8	68.6	63.4		

Dyke trends, where variable for individual dykes, are shown as local trend and overall trend (*within brackets*). Several dykes have notable curvatures in plan, and their overall trends are indicated by the "~" sign. Note that two of the analyses (CSD3 and CSD16) have totals exceeding 103 wt.%. The rock names and Mg Numbers (Mg#) for all samples are based on major oxide data recalculated to 100 % on an anhydrous basis using the SINCLAS program. Rock names are B, sa = subalkalic basalt, BA = basaltic andesite, PIC = picrite, A = andesite. Mg# = 100 $Mg^{2+}/(Mg^{2+}+Fe^{2+})$, atomic, where Fe^{2+} and Fe^{3+} are computed following Middlemost (1989). Reference values and measured values on the USGS standard BHVO2 (Wilson 2000) provide an idea about analytical accuracy

and Ivanov et al. (2008), respectively. Isotopic ratios were measured using a Finnigan MAT262 thermal ionization mass spectrometer. Accuracy of the analyses was tested by measurements on the reference materials SRM 987 (0.710263±0.000011, 2σ, n=10) and JNd-1 (0.512102±0.000005, 2σ, n=12).

Whole-rock samples of three of the longer and fresher aphyric dykes were dated by the $^{40}Ar/^{39}Ar$ incremental heating technique at the National Facility for $^{40}Ar/^{39}Ar$ Geochronology and Thermochronology, located in the Department of Earth Sciences, IIT Bombay. This employed a Thermo Fisher ARGUS mass spectrometer and the procedures described in Sen et al. (2012). The results are summarized in Table 4, and the stepwise analytical data are given in the Supplementary Table S2. The plateau spectra and isochron plots for the three samples are shown in Fig. 2. We define a plateau as comprising a minimum of 60 % of the total ^{39}Ar released and four or more successive degassing steps whose mean ages overlap at the 2σ level including the error contribution from the J value. The data were plotted using the program ISOPLOT v. 3.75 (Ludwig 2012).

Mineral compositions were obtained at Centro Interdipartimentale Strumentazioni per Analisi

Table 2 Trace element data (in ppm) for the Central Saurashtra dyke swarm and certified reference materials

Comp. Sample	B, sa CSD1	BA CSD3	BA CSD5	BA CSD6	PIC CSD8	PIC CSD9	B, sa CSD11	BA CSD15	B, sa CSD16	B, sa CSD17	B, sa CSD18	B, sa CSD19	BCR-2*m*	BCR-2*r*
Sc	36.1	32.0	32.0	31.6	36.1	36.6	48.0	29.4	46.8	33.1	35.7	37.3	32	33
V	284	479	471	273	266	268	343	155	322	261	258	300	416	416
Cr	860	213	349	477	623	690	442	375	646	389	613	398	20.2	18
Co	46.1	32.1	32.0	38.1	51.3	50.4	45.6	33.1	46.8	41.9	48.8	40.3	36.5	37
Ni	158	50.6	55.4	43	247	213	112	38.5	183	165	234	139	12.7	18
Cu	715	585	720	267	642	613	883	2231	1006	1252	1935	1908	23.5	19
Zn	480	347	441	251	415	382	547	1374	630	802	1250	1222	139	127
Ga	16.7	22.2	21.6	18.0	13.5	14.1	14.6	21.1	15.1	14.9	14.4	16.4	21.3	23
Ge	1.51	1.69	1.66	1.45	1.27	1.33	1.49	1.81	1.55	1.25	1.28	1.51	1.58	1.5
Rb	16.8	66.4	65.4	36.4	14.5	7.78	12.2	81.0	11.1	16.0	10.8	12.3	47.8	48
Sr	145	214	197	191	205	139	82.0	188	118	246	220	164	328	346
Y	25.0	50.9	50.9	25.2	20.6	17.3	23.7	57.2	22.8	21.6	21.1	23.3	37.6	37
Zr	101	312	294	137	69.5	43.3	29.5	320	56.6	73.4	68.2	101	204	188
Nb	5.32	41.5	38.5	7.85	10.7	5.21	3.57	37.9	9.68	12.0	11.2	10.6	13.3	12.6
Mo	3.30	2.29	3.36	2.35	1.54	1.97	2.21	3.57	2.81	1.93	1.83	2.23	235	248
Sn	18.1	13.0	16.0	7.47	15.3	14.2	19.5	52.4	23.4	30.8	49.6	47.6	2.23	2.47
Cs	0.26	0.70	0.94	0.26	0.16	0.07	0.07	1.90	0.17	0.29	0.45	0.63	1.14	1.1
Ba	111	414	397	187	147	86.3	43.5	421	105	165	154	125	678	683
La	10.2	40.5	39.7	16.1	9.21	3.10	3.36	44.2	6.35	10.2	9.94	11.8	24.1	25
Ce	21.5	82.1	80.1	34.4	18.8	6.81	7.27	89.4	13.4	20.7	20.0	24.2	52.6	53
Pr	2.79	9.45	9.22	4.14	2.35	0.95	1.03	10.3	1.71	2.56	2.46	3.07	6.44	6.8
Nd	12.5	38.3	37.4	17.2	10.0	4.56	5.01	42.1	7.60	10.7	10.4	13.0	27.6	28
Sm	3.41	8.61	8.36	4.21	2.55	1.67	1.82	9.46	2.14	2.73	2.64	3.37	6.39	6.7
Eu	1.08	2.41	2.35	1.27	0.90	0.69	0.69	2.55	0.77	0.94	0.89	1.04	1.94	2
Gd	4.15	9.40	9.25	4.73	3.11	2.36	2.68	10.5	2.82	3.27	3.20	3.86	6.91	6.8
Tb	0.68	1.42	1.42	0.73	0.53	0.43	0.51	1.59	0.53	0.54	0.54	0.63	1.04	1.07
Dy	4.28	8.49	8.52	4.39	3.40	2.85	3.64	9.48	3.63	3.57	3.50	3.91	6.36	6.41
Ho	0.89	1.78	1.78	0.92	0.75	0.62	0.85	1.98	0.81	0.78	0.76	0.82	1.3	1.33
Er	2.50	4.97	5.04	2.49	2.14	1.78	2.52	5.52	2.41	2.22	2.20	2.36	3.65	3.66
Tm	0.36	0.75	0.75	0.36	0.32	0.25	0.38	0.83	0.37	0.33	0.33	0.35	0.52	0.54
Yb	2.20	4.58	4.65	2.22	1.99	1.59	2.45	5.10	2.29	2.04	2.00	2.13	3.36	3.5
Lu	0.34	0.70	0.70	0.33	0.30	0.25	0.38	0.78	0.36	0.32	0.30	0.32	0.52	0.51
Hf	2.63	7.26	7.03	3.50	1.75	1.23	0.93	7.47	1.50	1.84	1.72	2.50	5.02	4.8
Ta	0.45	4.07	3.70	0.72	1.05	0.66	0.35	3.58	0.91	1.14	1.03	0.89	0.87	0.74
W	0.55	1.17	1.18	0.46	0.34	0.62	0.39	1.55	0.44	0.37	0.30	0.59	0.6	0.53
Pb	55.5	47.7	44.3	23.6	45.5	43.1	46.6	152	72.2	85.1	125	147	11.1	11
Th	3.20	10.2	9.91	4.32	1.63	0.73	0.52	12.1	0.86	1.71	1.68	3.15	5.89	6.2
U	0.76	2.21	2.22	0.99	0.24	0.10	0.08	2.60	0.18	0.26	0.25	0.67	1.58	1.69

r is the reference value (Wilson 1997), *m* the measured value on USGS standard BCR-2

Geomineralogiche, University of Naples, utilizing an Oxford Instruments Microanalysis Unit equipped with an INCA X-act detector and a JEOL JSM-5310 microscope. An accelerating voltage of 15 kV and a filament current of 50–100 mA was used for all the analyses. Measuring times were of 50 s. Silicates and oxides were used as standards (see Cucciniello et al. 2014 for details). The complete dataset of mineral analyses is available in the Supplementary Table S3.

Nomenclature and petrography

We used the SINCLAS program of Verma et al. (2002) to recalculate the major oxide compositions on a LOI-free basis and to obtain Mg Numbers [Mg# = 100 Mg/(Mg + Fe^{2+})], CIPW norms, and standardized, IUGS-recommended rock names (Le Bas et al. 1986; Supplementary Fig. 1) for the samples. Total iron was divided into Fe^{2+} and Fe^{3+} varieties

Table 3 Sr–Nd isotopic data for the Central Saurashtra dyke swarm

Comp.	Sample	$^{87}Rb/^{86}Sr$	$(^{87}Sr/^{86}Sr)_p$	±2σ	$(^{87}Sr/^{86}Sr)_t$	$^{147}Sm/^{144}Nd$	$(^{143}Nd/^{144}Nd)_p$	±2σ	$(^{143}Nd/^{144}Nd)_t$	εNd_t
B, sa	CSD1	0.34	0.714522	0.000012	0.714212	0.17	0.512205	0.000012	0.512135	–8.2
BA	CSD3	0.90	0.708352	0.000015	0.707521	0.14	0.512426	0.000010	0.512368	–3.6
BA	CSD5	0.96	0.708435	0.000014	0.707547	0.13	0.512422	0.000007	0.512365	–3.7
BA	CSD6	0.55	0.717556	0.000014	0.717048	0.15	0.511988	0.000007	0.511925	–12.3
PIC	CSD8	0.20	0.707285	0.000015	0.707096	0.15	0.512488	0.000007	0.512422	–2.6
PIC	CSD9	0.16	0.706407	0.000014	0.706257	0.22	0.512567	0.000016	0.512473	–1.6
B, sa	CSD11	0.43	0.705355	0.000014	0.704956	0.22	0.512863	0.000009	0.512770	+4.2
BA	CSD15	1.25	0.709673	0.000013	0.708520	0.14	0.512346	0.000010	0.512288	–5.2
B, sa	CSD16	0.27	0.705430	0.000014	0.705179	0.17	0.512693	0.000012	0.512621	+1.3
B, sa	CSD17	0.19	0.707399	0.000016	0.707225	0.15	0.512498	0.000012	0.512432	–2.4
B, sa	CSD18	0.14	0.707200	0.000015	0.707068	0.15	0.512512	0.000016	0.512447	–2.1
B, sa	CSD19	0.22	0.708019	0.000016	0.707819	0.16	0.512434	0.000007	0.512367	–3.6

Comp. indicates composition (rock type) as in Tables 1 and 2. The Sr and Nd isotopic measurements were on unleached samples. Subscripts "p" and "t" on Sr and Nd isotopic ratios and εNd values indicate present-day and initial (age-corrected to 65 Ma) values, respectively

based on the Middlemost (1989) scheme offered by SINCLAS. The Central Saurashtra dykes range in composition from picrite (with >12 wt.% MgO) to basalt, basaltic andesite, and andesite (Table 1). All samples are subalkalic with normative hypersthene (4.06–27.3 wt.%), and several samples have normative quartz (from 1.57 wt.% to as much as 18.0 wt.% in the andesite CSD13).

The picrites (e.g. CSD8 and CSD9) have subophitic or porphyritic textures (Supplementary Fig. 2a, b). Phenocrysts commonly make up 15–20 % and rarely exceed 30 % by volume of the picrites. Olivine occurs as phenocrysts, microphenocrysts, or microlites in the groundmass. Olivine phenocrysts and microphenocrysts are euhedral or subhedral, zoned, generally altered along fractures to iddingsite and often contain small rounded spinel inclusions (Supplementary Fig. 2a, b). Clinopyroxene forms euhedral to subhedral phenocrysts or microphenocrysts, or subophitic or intergranular phases in the groundmass (Supplementary Fig. 2a, b). Plagioclase forms euhedral to subhedral lath-shaped crystals (Supplementary Fig. 2a, b). Opaque oxides occur as microphenocrysts or microlites. Apatite is an accessory groundmass phase.

The basaltic dykes (Supplementary Fig. 2c–f) are porphyritic with phenocrysts of olivine and subordinate clinopyroxene constituting 10–20 % by volume, but some samples show a subophitic texture. They consist of subhedral or rounded olivine (always altered to iddingsite along fractures), subhedral, interstitial, or oikocrystic clinopyroxene, euhedral to subhedral lath-shaped plagioclase, and interstitial anhedral opaque oxides. Chromiferous spinels are enclosed in olivine phenocrysts and sometimes also in clinopyroxene grains. Pigeonite is found at boundaries of clinopyroxene grains, or within the groundmass (Supplementary Fig. 2f). Orthopyroxene has been found only in the sample CSD18 as a late-crystallized phase in the groundmass with quartz, alkali feldspar, pigeonite, and opaque oxides (Supplementary Fig. 2f). Interstitial glass (of rhyolitic composition) is rarely observed (CSD1). The Sardhar basaltic andesite (CSD5) is a fine-grained rock with microphenocrysts of plagioclase and clinopyroxene in a groundmass of plagioclase, quartz, clinopyroxene, pigeonite, and opaque oxides (Supplementary Fig. 2 g, h).

Table 4 Summary of $^{40}Ar/^{39}Ar$ dating results for the Central Saurashtra dykes

Sample	Plateau					Isochron				Inverse isochron			
	Steps	$\%^{39}Ar$	Age (Ma)	MSWD	*p*	Age (Ma)	Trap	MSWD	*p*	Age (Ma)	Trap	MSWD	*p*
CSD5	17	95.4	65.6±0.2	0.58	0.90	65.6±0.3	296.4±2.3	0.21	0.99	65.6±0.3	296.6±1.7	0.51	0.94
CSD8	12	77.9	66.6±0.3	0.77	0.67	66.5±0.6	295.6±2.1	0.08	1.00	66.4±0.4	296.0±1.6	0.26	0.99
CSD11	11	70.4	62.4±0.3	0.61	0.81	62.4±0.5	295.2±3.3	0.13	0.99	62.5±0.3	295.0±2.0	0.61	0.79

Trap is initial $^{40}Ar/^{36}Ar$ ratio (trapped component), MSWD is mean square weighted deviate, and *p* is the corresponding probability. Errors are reported at the 2σ confidence level and monitor mineral is MMHb (523.1±2.6 Ma; Renne et al. 1998). Interference corrections for Ca- and K-produced Ar isotopes based on analysis of CaF_2 and K_2SO_4 salts were $(^{36}Ar/^{37}Ar)_{Ca}$, $(^{39}Ar/^{37}Ar)_{Ca}$, and $(^{40}Ar/^{39}Ar)_K$=0.000344, 0.001062, and 0.0006466, respectively. ^{40}Ar blank contributions were 1–2 % or less for all temperature steps. The irradiation parameter *J* for each sample was corrected for neutron flux variation using the activity of nickel wires irradiated with each sample. Values of fluence-corrected *J* for various samples are as follows: CSD5, 0.002216±0.000009; CSD8, 0.002308±0.000009; and CSD11, 0.002180±0.000009.

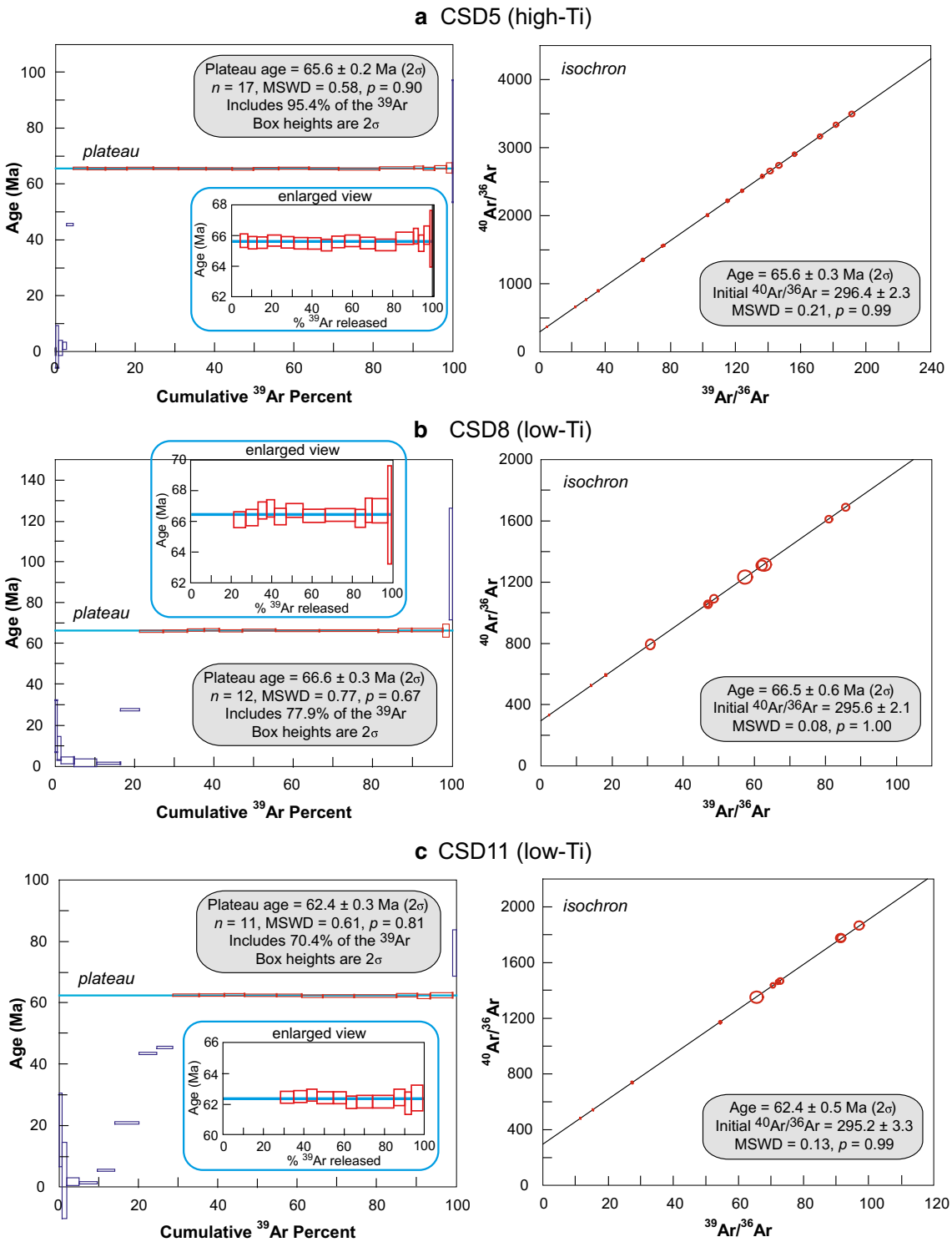

Fig. 2 $^{40}Ar/^{39}Ar$ plateau spectra (*left panels*) and isochron plots (*right panels*) for the Central Saurashtra dyke samples **a** CSD5, **b** CSD8, and **c** CSD11. In the plateau spectra, the plateau steps are shown with *red* outlines and the nonplateau steps with *dark blue* outlines. Also shown are values of the mean square weighted deviate (*MSWD*) and probability (*p*). *Inset* figures show the enlarged views of the plateau spectra

$^{40}Ar/^{39}Ar$ dating

The three dated samples (sample CSD5 from the N87°-trending Sardhar basaltic andesite dyke, sample CSD8 from a N77°-trending picrite dyke, and sample CSD11 from a N113°-trending basalt dyke) yielded very good plateau spectra (Fig. 2a, b, c). Also, the concordant plateau, isochron and inverse isochron ages for each sample, the large amounts of

total released ^{39}Ar (70.4–95.4 %) for the plateau steps, the acceptable mean square weighted deviate (MSWD) values of the isochrons and inverse isochrons, as well as the atmospheric $^{40}Ar/^{36}Ar$ ratio (295.5) of the trapped argon given by their intercepts (Fig. 2a, b, c), suggest that these ages represent true crystallization ages. We therefore take the plateau ages as the crystallization ages. The dyke CSD5 has an age of 65.6± 0.2 Ma (2σ), dyke CSD8 has an age of 66.6±0.3 Ma (2σ), and dyke CSD11 has an age of 62.4±0.3 Ma (2σ). The first two ages are essentially the same as those determined for the bulk of the Deccan Traps (e.g., Baksi 2014 and references therein).

Mineral chemistry

Olivines

Olivine has a wide range of composition from Fo_{84} to Fo_{51} in picrites and from Fo_{85} to Fo_{18} in tholeiitic basalts (where Fo = 100 Mg/(Mg + Fe); Supplementary Fig. 3a). MnO in olivine ranges from 0.1 to 1.4 wt.%. NiO ranges from below detection limits to 0.7 wt.% and tends to decrease with decreasing MgO. CaO ranges from 0.1 to 0.8 wt.% (Supplementary Table S3).

Pyroxenes

Clinopyroxenes of the Central Saurashtra dykes belong to the augite–ferroaugite and diopside–hedenbergite series (nomenclature of Morimoto et al. 1988; Supplementary Table S3; Supplementary Fig. 3b). The first series occurs in the basaltic samples CSD1, CSD5, and CSD18 ($En_{46}Fs_9Wo_{45}$ to $En_{32}Fs_{41}Wo_{27}$) and shows Fe enrichment and Ca depletion from clinopyroxene cores to rims and with increasing differentiation. TiO_2 and Al_2O_3 contents are low (0.3–1.6 wt.% TiO_2 and 1.0–3.7 wt.% Al_2O_3). Pigeonite is relatively abundant in the groundmass of these samples. It has a compositional range from $En_{50}Fs_{40}Wo_{10}$ to $En_{22}Fs_{63}Wo_{15}$. Fe-rich orthopyroxene ($En_{27}Fs_{70}Wo_3$) has been found in the tholeiitic dyke CSD18. Equilibration temperatures of groundmass clinopyroxenes and pigeonites in the Mg-rich basaltic dyke CSD18 and the basaltic andesite CSD5, based on the two-pyroxene geothermometer of Lindsley (1983), range from 1100 to 1000 °C. Similar temperatures (~1059–961 °C) are obtained for groundmass pigeonites using the algorithm of Ishii (1975). Temperatures calculated using equilibrium clinopyroxene phenocrysts or microphenocrysts and the Putirka (2008) clinopyroxene-liquid geothermometer range from ~1200 °C for the Mg-rich basaltic dyke CSD18 to ~1100 °C for the basaltic andesite CSD5. Clinopyroxenes in the picrites and some of the basalts (CSD7, CSD16, and CSD17) fall in the diopside–hedenbergite field close to augite–ferroaugite boundary ($En_{46}Fs_9Wo_{45}$ to $En_{17}Fs_{39}Wo_{43}$). Their Mg# values [where Mg# = 100 Mg/(Mg + Fe)] range from 83 to 31. TiO_2 and Al_2O_3 range from 0.3 to 2.7 and from 2.0 to 6.2 wt.%, respectively. Clinopyroxenes belonging to the diopside–hedenbergite series have been also observed in the transitional lavas of Pavagadh (e.g., Sheth and Melluso 2008) and in some Gujarat basalts with weakly alkaline affinity (e.g., Melluso et al. 1995, 2006; Krishnamurthy et al. 2014; Supplementary Fig. 3b). The clinopyroxene compositions of the Central Saurashtra picrite dykes plot well within the field defined by clinopyroxenes of the more primitive NE Saurashtra drillhole lavas (Krishnamurthy and Cox 1977; Supplementary Fig. 3b).

Feldspars

Feldspars in the Central Saurashtra dykes have been classified following the method of Deer et al. (2001). Plagioclase in the picrites and basaltic dykes varies from bytownite ($An_{85–69}$) to oligoclase ($An_{29–19}$). Alkali feldspar ($Or_{14–61}$) is rare and occurs in the groundmass (Supplementary Table S3; Supplementary Fig. 3c). In the basaltic andesite CSD5, plagioclase varies from labradorite (An_{56}) to andesine (An_{36}). The feldspars analyzed in all Central Saurashtra dykes plot well within the field of feldspars of other Deccan Traps rocks (Supplementary Fig. 3c).

Oxides

Magnetite is the main oxide mineral in the Central Saurashtra dykes. The ulvöspinel concentration of magnetite ranges from 49 to 77 mol % in the picrites and from 41 to 88 mol % in the basaltic dykes (Supplementary Table S3; Supplementary Fig. 3d). Al_2O_3 is variable (0.7–4.1 wt.%). Ilmenite usually cocrystallizes with magnetite in the Central Saurashtra dykes. It is homogeneous in composition ($ilm_{91–97}$) and has low Al_2O_3 (<0.4 wt %) and MnO (0.3–1.1 wt %) contents (Supplementary Table S3). Equilibrium temperatures and oxygen fugacities of coexisting magnetite and ilmenite, calculated using the ILMAT program of Lepage (2003), range from 1141 to 845 °C and from −15 to −10logfO_2 units in the picrites, and from 1100 to 671 °C and from −20 to −10logfO_2 units in the basaltic rocks. These values plot close to the quartz–fayalite–magnetite (QFM) buffer and are similar to the values reported by Melluso and Sethna (2011) for other Deccan Traps rocks. Chromiferous spinel occurs as small inclusions in olivine phenocrysts and microphenocrysts. The compositional range observed is wide with Al_2O_3 varying from 35.1 to 11.1 wt.%, Cr_2O_3 varying from 42.3 to 23.8 wt.% (Cr#=64-32; where Cr#=100Cr/(Cr + Al)), and MgO varying from 14.0 to 4.1 wt.% (Mg#=63-19; Supplementary Table S3). The most Cr-rich spinels have been found in the basaltic dykes (e.g., CSD1 and CSD18). In the Cr–Al–(Fe^{3+}+2Ti) diagram (Supplementary Fig. 3e), data for the chromiferous spinels of the Central Saurashtra dykes plot within the field of spinels of other Deccan Traps rocks (Melluso and Sethna 2011).

Whole-rock geochemistry

Alteration effects on whole-rock composition

The majority of the Central Saurashtra dykes have values of loss on ignition (LOI) below 1.5–1.8 wt.% (and well below 1.0 wt.% for several), suggesting that the samples are relatively fresh (consistent with petrographic observations), and their analyzed major and trace element and Sr–Nd isotopic compositions reflect magmatic compositions. However, this may not be true of Pb concentrations. Compared to the common 2–5 ppm Pb concentrations in Deccan lavas and dykes (e.g., Peng et al. 1994, 1998, 2014; Vanderkluysen et al. 2011), the Central Saurashtra dykes have Pb concentrations ranging from 23.6 ppm (CSD6) to as much as 152 ppm (CSD15). Similar or higher Pb concentrations observed in the highly weathered lavas and dykes from eastern Saurashtra and Mumbai areas were ascribed to probable hydrothermal alteration (Sheth et al. 2013, 2014). This explanation is unlikely for the Central Saurashtra dykes, and we suspect that the very high Pb values reflect contamination, from an unidentified source, during the preparation of sample powders. We therefore do not use the Pb data in this paper and use only the alteration-resistant elements (Ti, Zr, Nb, Y, Th, and the REE) and their ratios, as well as isotopic ratios (particularly of Nd) for geochemistry-based modeling and interpretations.

Major and trace elements

The whole-rock major and trace element data for the Central Saurashtra dykes are presented in Tables 1 and 2. The picrites have MgO contents between 15.6 and 12.4 wt.%, and Mg# values of 75–69. MgO content of the basaltic dykes ranges from 11.5 to 8.5 wt.% and the Mg# varies from 68 to 62 (Table 1). The Ni and Cr contents (Ni=247–183 ppm; Cr=860–613 ppm) of the picritic and Mg-rich basaltic dykes are within the ranges expected for mantle-derived melts (but see below). Unlike three basaltic andesites (CSD3, 5, and 15) and one andesite (CSD13) with 2.8–3.2 wt.% TiO_2, the picrites and basalts have low concentrations of the immobile high field strength elements such as TiO_2 (0.7–1.3 wt.%), P_2O_5 (0.1–0.2 wt.%), and Zr (30–101 ppm). They have moderate Zr/Nb (6–19) and Lu/Hf (0.1–0.4), and low Zr/Y (1–4) and Ti/V (13–26) typical of enriched mid-ocean ridge basalt (E-MORB) magmas (e.g., Sun and McDonough 1989).

Flood basalts of the world have often been classified into low-Ti and high-Ti types which cannot be related by fractional crystallization but require distinct parental magmas (e.g., Hergt et al. 1991; Peate 1997; Shellnutt et al. 2014). Based on

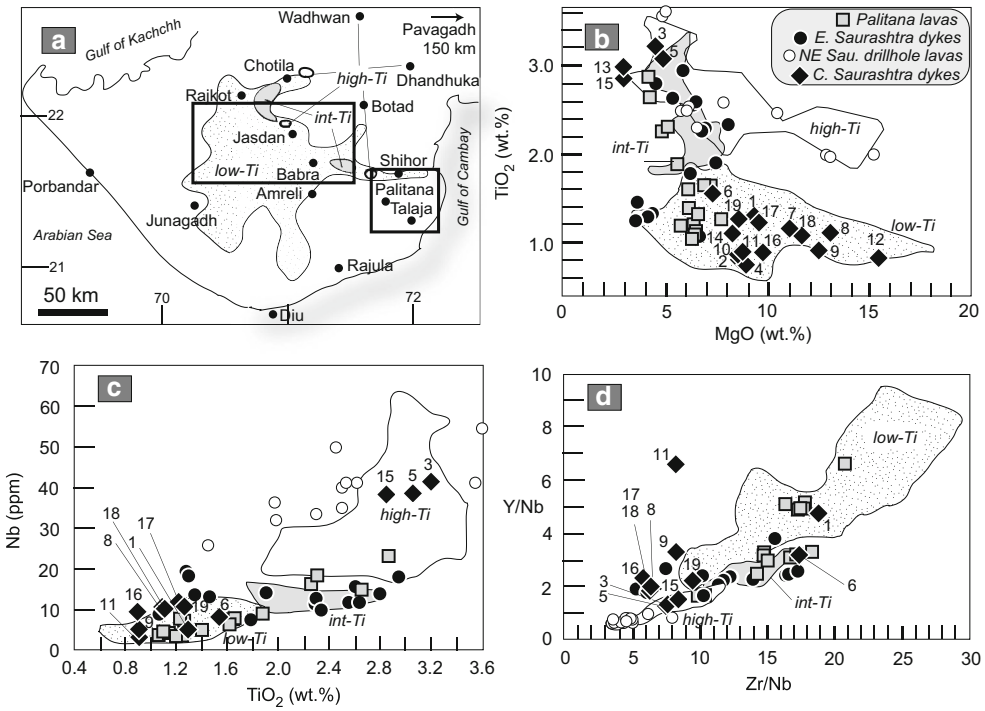

Fig. 3 **a** Map of Saurashtra showing the distribution of the high-Ti, intermediate-Ti, and high-Ti basalt surface outcrops (based on Melluso et al. 1995). The drillhole lavas of Wadhwan, Dhandhuka, and Botad are also high Ti, as are lavas of Pavagadh 150 km east of Wadhwan. **b**, **c**, **d** Classification of the Central Saurashtra dyke samples into the three Ti types, using the criteria and fields of Melluso et al. (1995). Specific samples discussed in the text are indicated. Also plotted are data for the NE Saurashtra drillhole lavas (Krishnamurthy and Cox 1977) and the Palitana lavas and Eastern Saurashtra dykes (Sheth et al. 2013). Note from (**b**) that whereas a few Central Saurashtra dykes are as evolved as the Palitana lavas and Eastern Saurashtra dykes, many Central Saurashtra dykes are much less evolved. The data point for CSD11 plots as an outlier in panel (**d**). This is because of the anomalously low Zr (29 ppm) and Hf (0.93 ppm) measured for CSD11 (Table 2), probably caused by incomplete sample digestion

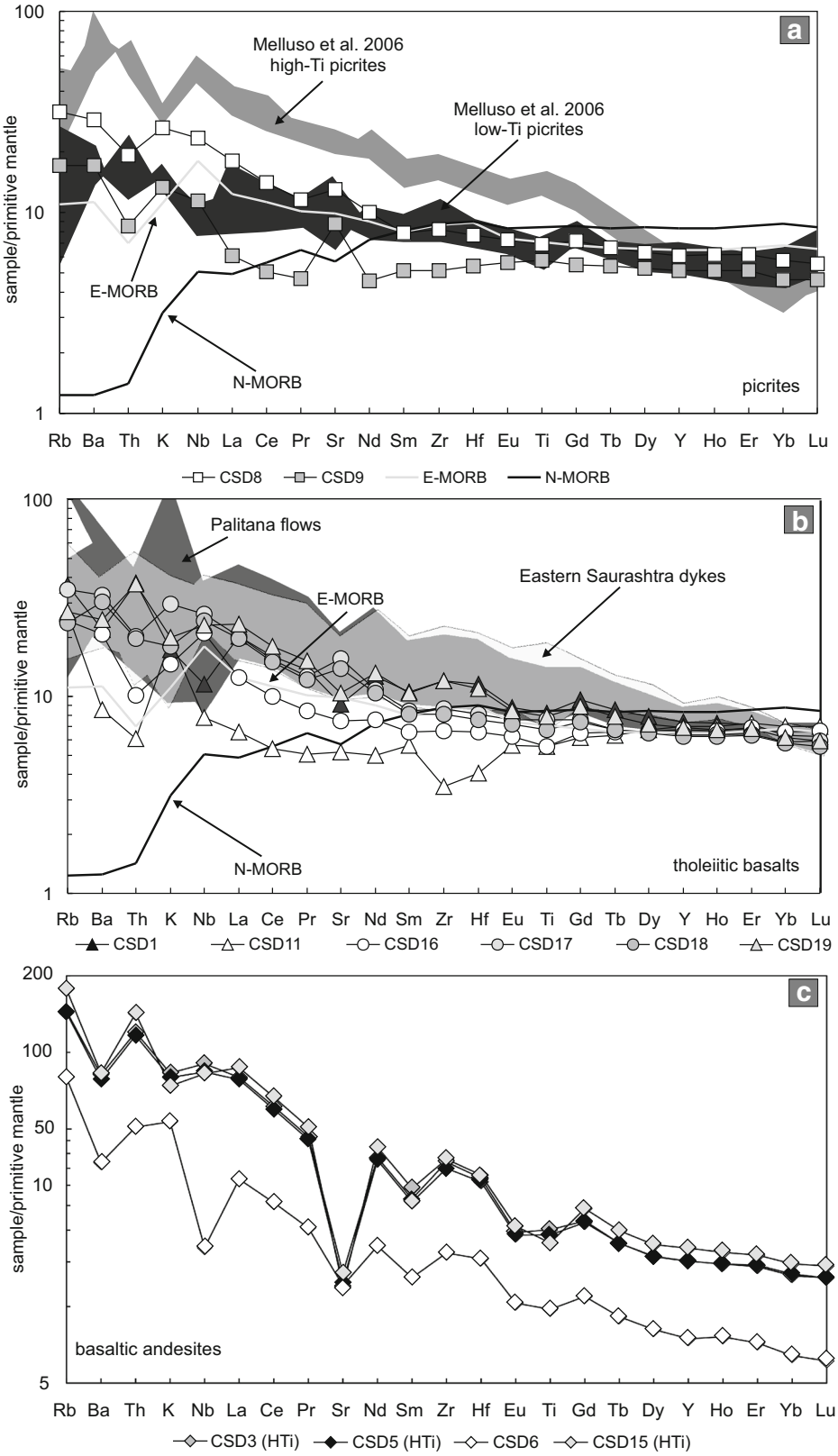

Fig. 4 Primitive mantle-normalized incompatible element patterns for the Central Saurashtra dykes. **a** Picrites. **b** Basalts. **c** Basaltic andesites. The normalizing values are from Lyubetskaya and Korenaga (2007). Fields for Palitana flows and Eastern Saurashtra dykes (Sheth et al. 2013) and the Saurashtra low-Ti and high-Ti picritic flows (Melluso et al. 2006) are also shown for comparison. N-MORB and E-MORB patterns are plotted with the values of Sun and McDonough (1989)

combined TiO_2 and Nb contents and Zr/Y and Ti/Y ratios, Melluso et al. (1995) classified the Deccan rocks of Saurashtra into low-Ti, high-Ti, and intermediate-Ti types, with 1.8 wt.% TiO_2 as the upper limit for the low-Ti type (Fig. 3). The low-Ti rocks have Nb<10–12 ppm (mostly <9 ppm), even when highly evolved, and low Zr/Y (average 3.7) and low Ti/Y (average 281) ratios. Based on their scheme, Sheth et al. (2013) found that the Palitana lava flows are dominantly low-Ti with a few high-Ti and intermediate-Ti members, and the Eastern Saurashtra dykes include all three types. The NE Deccan drillhole sequences (and the Pavagadh basalts further east) are high-Ti (Melluso et al. 2006; Sheth and Melluso 2008). We find that the Central Saurashtra dykes are dominantly low-Ti, with four samples (CSD3, 5, 13, and 15) being high-Ti and the intermediate-Ti type absent (Fig. 3). The high-Ti rocks are considerably more evolved than the rest of the suite, with MgO < 5 wt.% and Mg# ranging from 48.0 to as low as 32.3 (Table 1).

Primitive mantle-normalized multielement patterns of the Central Saurashtra mafic dykes (picrites and basalts, excluding basalt CSD11) are variably enriched in Rb, Ba, and the LREE relative to Zr, Hf, Ti, and the HREE (Fig. 4a, b). The patterns are relatively flat with low normalized abundances from Eu to Lu (less than ten times primitive mantle values) and show no Nb anomalies (excluding the basalt CSD1 with a marked negative Nb anomaly). In some samples (e.g. CSD8, CSD16, and CSD18), the concentrations of many elements are similar to those in average E-MORB (Sun and McDonough 1989). Primitive mantle-normalized incompatible element patterns of the high-Ti basaltic andesites (CSD3, 5, and 15) show marked troughs at Ba and Sr and peaks at Th (Fig. 4c). The pattern of the low-Ti basaltic andesite CDS6 displays a marked trough at Nb, a weak trough at Sr and lower normalized abundances than the high-Ti basaltic andesites.

Sr and Nd isotopic ratios

Strontium and neodymium isotopic ratios for 12 Central Saurashtra dykes, corrected for an age of 65 Ma, are reported in Table 3 (age correcting the isotopic ratios for sample CSD11 to 62.4 Ma makes little difference). Of these 12 dykes, ten show a range of $(^{87}Sr/^{86}Sr)_t$ from 0.70496 to 0.70852 and $(^{143}Nd/^{144}Nd)_t$ from 0.512863 ($\varepsilon_{Nd}t$=+4.2) to 0.512346 ($\varepsilon_{Nd}t$=–5.2; Fig. 5). The isotopic ratios correlate with the degree of LREE enrichment ($^{143}Nd/^{144}Nd$ decreases with increasing La/Sm ratio). Two dykes (basalt CSD1 and basaltic andesite CSD6) have

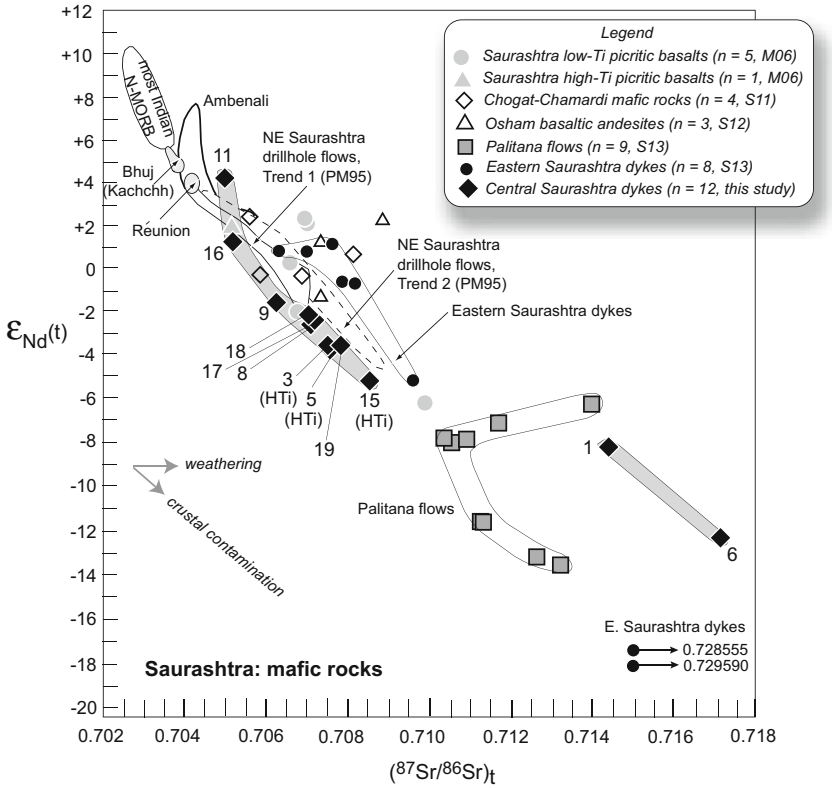

Fig. 5 Sr–Nd isotopic plot for the Central Saurashtra dykes, with sample numbers marked. Data are shown for other Saurashtra mafic suites including the Palitana lavas and the Eastern Saurashtra dykes, the Saurashtra low-Ti and high-Ti picritic flows including the NE Saurashtra drillhole lavas, the Osham Hill basaltic andesite lavas, and the Chogat-Chamardi gabbros and mafic dykes. Data sources are: PM95, Peng and Mahoney (1995); M06, Melluso et al. (2006); S11, S12, and S13: Sheth et al. (2011, 2012, and 2013). All data are initial values for 65 Ma. The NE Saurashtra high-Ti drillhole lavas define the separate "Trend 1" and "Trend 2" which, while showing significant overlap here, are well resolved on Nd–Pb and Sr–Pb isotopic plots (Peng and Mahoney 1995). Fields for Indian N-MORB, Bhuj area mafic alkalic rocks, and Réunion lavas are also shown for comparison (Peng and Mahoney 1995)

highly radiogenic ($^{87}Sr/^{86}Sr)_t$ (0.71421 and 0.71705, respectively) and highly unradiogenic ($^{143}Nd/^{144}Nd)_t$ (0.512205 and 0.511988, corresponding to $\varepsilon_{Nd}t$=−8.2 and −12.3, respectively; Fig. 5). The Central Saurashtra dykes have similar Nd isotopic ratios to the Eastern Saurashtra dykes ($\varepsilon_{Nd}t$=+1.1 to −5.2 for six samples, with two other samples having $\varepsilon_{Nd}t$=−17.4 and −18.0; Sheth et al. 2013). However, the Central Saurashtra dykes have systematically lower Sr isotopic ratios than the Eastern Saurashtra dykes (0.70635–0.72959). This difference cannot be explained by the significantly weathered nature of the latter, because the isotopic data for both swarms define strongly anticorrelated and well-separated arrays, whereas any disturbance of the isotopic ratios by weathering would have resulted in at least some overlap between both arrays. We interpret this as indicating petrogenetically independent magmatic evolution in both dyke swarms.

Magmatic evolution

The entirely subalkalic Central Saurashtra dykes show a considerable variation in major element composition (ranging from picrite to andesite), trace element (including REE) contents, and Sr–Nd isotopic ratios. We now discuss mechanisms to generate these variations, including fractional crystallization and crystal accumulation, and crustal contamination.

Fractional crystallization and crystal accumulation

Petrographic features and major and trace element variations observed in the Central Saurashtra dykes (e.g. 46.4–55.4 wt.% SiO_2) are consistent with fractional crystallization and crystal accumulation processes. The dykes show significant variations in SiO_2, TiO_2, Al_2O_3, and CaO with MgO (Fig. 6a–d). Ni and Cr are strongly correlated with MgO, suggesting fractional crystallization of olivine + Cr-spinel (Fig. 6e, f). Al_2O_3 and CaO first increase with decreasing MgO and begin to decrease when MgO reaches 9 wt.% (Fig. 6c, d), suggesting fractionation of clinopyroxene and plagioclase. However, some dykes (CSD1, 2, 4, 12, 14, 16, and 19) show higher Al_2O_3 and lower CaO and Sc contents, for a given MgO content, than the other dykes. This characteristic is not due to excess plagioclase (as none of the samples show plagioclase phenocrysts in thin section) and may suggest higher pyroxene:plagioclase ratios in the fractionation assemblages or different parental magmas. Incompatible trace elements, such as Rb and Zr, also show negative correlation with MgO (Fig. 6g, h).

An important question is whether the Central Saurashtra picrites are high-MgO liquids or cumulus-enriched rocks. Picritic rocks in the NE Saurashtra drillholes have been interpreted as near-primary liquids with ~16 wt.% MgO (West 1958; Krishnamurthy and Cox 1977; Krishnamurthy et al. 2000), whereas most picritic rocks in the Western Ghats sequence appear to be evolved basaltic liquids which have accumulated olivine and clinopyroxene (Beane and Hooper 1988), with such accumulation reaching an extreme level in the Khopoli olivine gabbro (Cucciniello et al. 2014). We plotted the olivine compositions (Fo %) in Central Saurashtra picrites CSD8 and CSD9 against their whole-rock Mg# values (Fig. 7). The olivine compositions plot well below the equilibrium K_d band (drawn using a Fe/Mg K_d=0.30±0.03; Roeder and Emslie 1970), implying forsterite contents too low to be in equilibrium with the whole-rock Mg# (69–70) values. The most Mg-rich olivine compositions (Fo_{84} in CSD8) would have been in equilibrium with a melt with Mg#=64. This means that cumulus enrichment of low-Fo olivines has raised the bulk-rock MgO contents and Mg# values, and the resultant picritic rocks do not represent high-MgO liquids (cf. Cucciniello et al. 2014; Chatterjee and Sheth 2015). In fact, olivine compositions of five of the tholeiitic dykes also plot below or well below the equilibrium K_d band (Fig. 7), suggesting that cumulus enrichment of olivine phenocrysts (or xenocrysts) was a widespread process in the Central Saurashtra dyke magmas.

To model the effects of fractional crystallization on major element compositions, we performed mass balance calculations (Stormer and Nicholls 1978) on pairs of samples from the same dykes (or from dykes located nearby). Thus, for the Isapur-Charkha dyke (Fig. 1c), ~6 % olivine fractionation from the picrite CSD8 generates the basalt CSD7 ($\sum R^2$=0.45). The transition from basalt dyke CSD16 to the nearby basaltic dyke CSD14 is modeled by 35 % fractional crystallization of olivine (12 %), clinopyroxene (54 %), plagioclase (28 %), and magnetite (6 %; $\sum R^2$=0.22). The transition from basalt dyke CSD19 to the nearby basaltic andesite dyke CSD15 is modeled by 61 % fractional crystallization of olivine (17 %), clinopyroxene (40 %), and plagioclase (43 %; $\sum R^2$=0.25). For the transition from basalt CSD1 to basaltic andesite CSD5 in the Sardhar dyke, the extract removed (62 %) is composed of olivine (22 %), plagioclase (42 %) and clinopyroxene (36 %; $\sum R^2$=0.37). For the transition from basalt CSD1 to basaltic andesite CSD6, the extract removed (58 %) is composed of olivine (24 %), plagioclase (52 %), and clinopyroxene (24 %; $\sum R^2$=0.42). The mass balance calculations are in agreement with the observed mineral assemblages.

Crustal contamination

Fractional crystallization and crystal accumulation processes (and prior partial melting processes) cannot have generated the variability observed in the incompatible element ratios and the Sr–Nd isotopic ratios of the Central Saurashtra dykes. Therefore, these variations must reflect open-system processes, most importantly contamination of the dyke magmas by lithospheric materials. Trace element ratios, such as Nb/U, Th/Nb, and La/Nb, and radiogenic isotope ratios (e.g., $^{87}Sr/^{86}Sr$ and $^{143}Nd/^{144}Nd$) are commonly used to assess the role of crustal contamination because of the strongly contrasted compositions

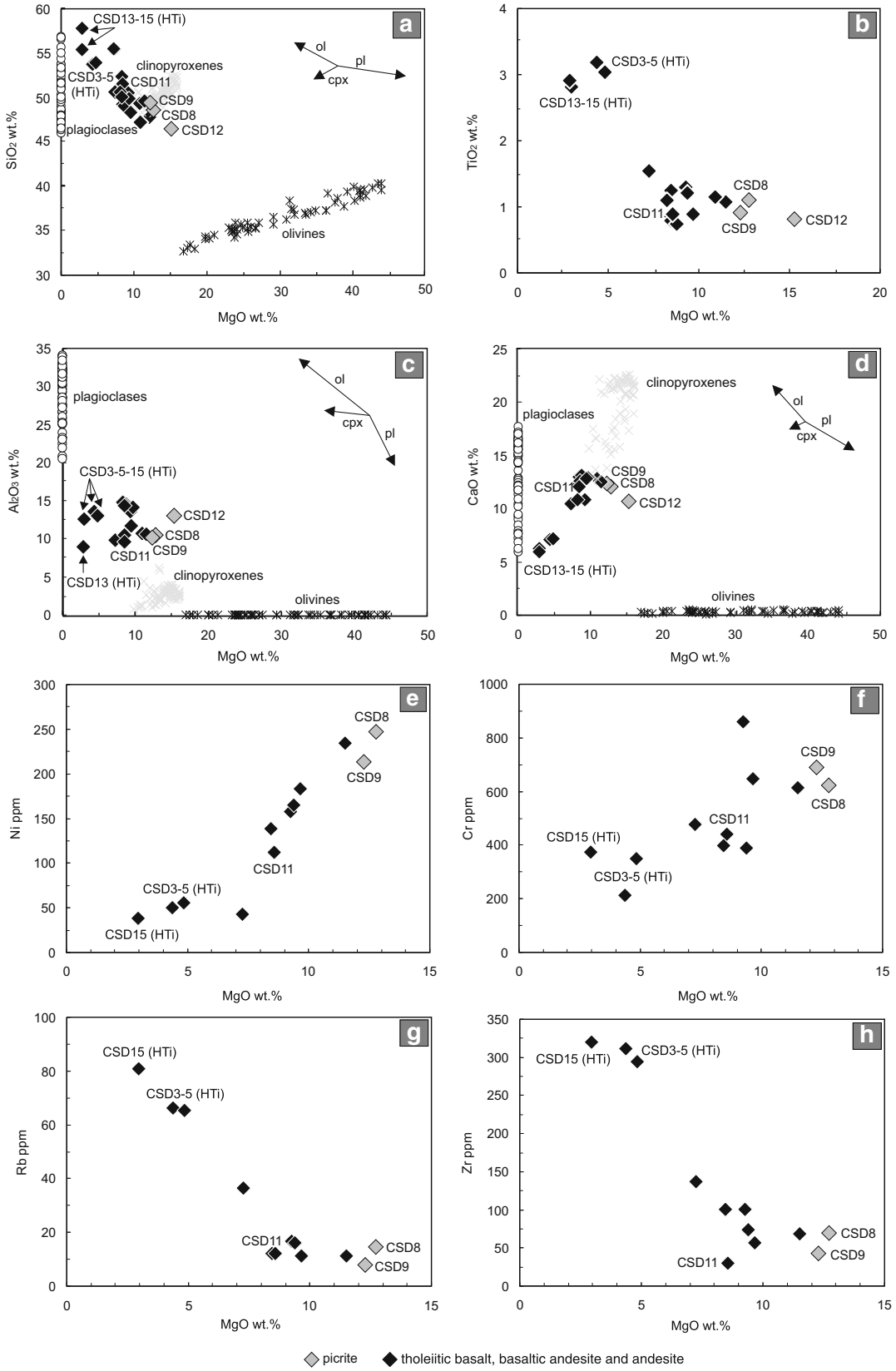

Fig. 6 **a**–**h** Whole-rock major oxide (wt.%) and trace element (ppm) variations among the Central Saurashtra dykes (12 samples). The mineral phases of Central Saurashtra dykes and the crystallization vectors of olivine, clinopyroxene, and plagioclase are indicated on the diagrams of SiO_2, Al_2O_3, and CaO vs. MgO. The high-Ti dykes are indicated and the rest are all low-Ti

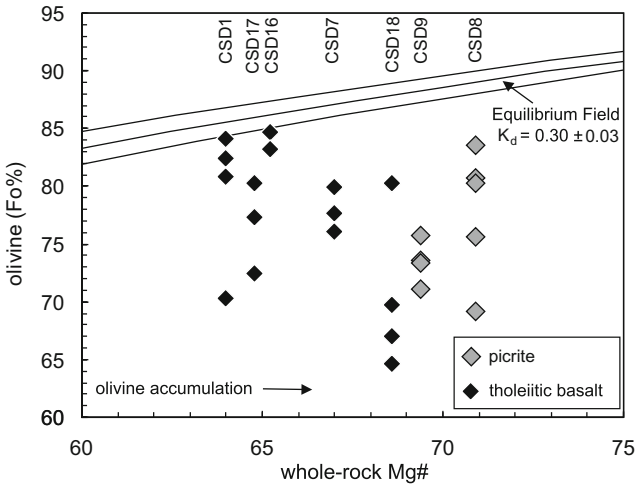

Fig 7 Whole-rock Mg Number (Mg#) vs. olivine phenocryst core composition (Fo %) for the Central Saurashtra dykes. The equilibrium field, bounded by the three curves, represents the Fe–Mg partition coefficient between olivine and liquid (K_d=0.30±0.03; Roeder and Emslie 1970)

of mantle-derived mafic magmas and continental crustal materials. Ocean island basalt (OIB) and MORB (e.g., E-MORB and N-MORB) have high Nb/U (>45) and low La/Nb (0.8–1.1) and Th/Nb (<0.1) ratios (e.g., Sun and McDonough 1989). The continental crust has lower Nb/U (4.4–25) and higher La/Nb (1.6–2.6) and Th/Nb (0.24–0.88) ratios than MORB and ocean island basalts (e.g., Rudnick and Gao 2003).

The Central Saurashtra picrites and most basaltic dykes have Nb/U (45–54), Th/Nb (0.09–0.15), and La/Nb (0.6–0.9) ratios similar to MORB and OIB, suggesting little or no crustal contamination. In contrast, the basalts CSD1 and CSD19 and the basaltic andesites have lower Nb/U (8–17) and higher La/Nb (1.0–2.1) and Th/Nb (0.25–0.6) ratios trending toward crust-like compositions. Plots of $\varepsilon_{Nd}t$ and the alteration-resistant incompatible trace element ratios Th/Nb, La/Nb, and Zr/Nb (Fig. 8a, b, c) show that the Central Saurashtra dyke data plot along broad crustal contamination trends which are parallel or subparallel to the arrays defined by the Palitana and Eastern Saurashtra dykes (Sheth et al. 2013). Notably, the Central Saurashtra dykes mostly lie along the lower ends of the overall mixing arrays, with the exception of basalt CSD1 and basaltic andesite CSD6 (having $\varepsilon_{Nd}t$=–8.2 and –12.3, respectively, suggesting much higher degrees of crustal contamination). The elongation of the individual arrays also suggests that two-component mixing between mantle-derived magmas and a single crustal end member may not be adequate and that several mixing end members may have been involved.

Figure 9 is a plot of Ti/Y vs. Zr/Nb, employing four elements that are highly alteration-resistant, and these ratios are insensitive to crystal fractionation of the main basaltic minerals. Crustal contamination of mafic magmas would raise their Zr/Nb while lowering Ti/Y. Most Central Saurashtra dykes form a distinct cluster

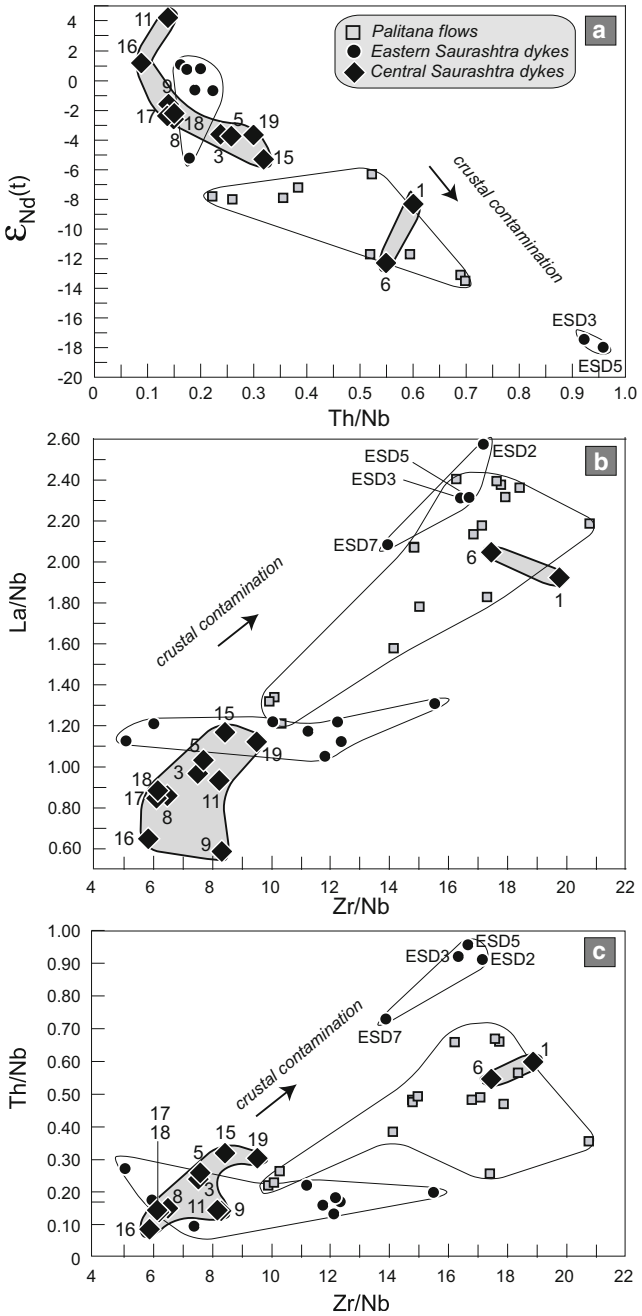

Fig. 8 Plots of initial **a** ε_{Nd} vs. Th/Nb, **b**–**c** La/Nb and Th/Nb vs. Zr/Nb for the Central Saurashtra dykes. The data for the Palitana flows and the Eastern Saurashtra dykes (Sheth et al. 2013) are also shown. The trends expected from crustal contamination are indicated by the *arrows*

from not only the Western Ghats lavas but also all other Saurashtra mafic rocks including the NE Saurashtra drillhole lavas, the Palitana lavas, and the Eastern Saurashtra dykes (Fig. 9). Most of the Central Saurashtra dyke data (with small negative $\varepsilon_{Nd}t$ values) plot at the lower left end of the diagram, indicating that they have been contaminated to low degrees. On the other hand, data for dykes CSD1 and CSD6 plot at much higher Zr/Nb, overlapping with the highly crustally contaminated Bushe Formation of the Western Ghats sequence (e.g., Beane et al. 1986). Dykes CSD1

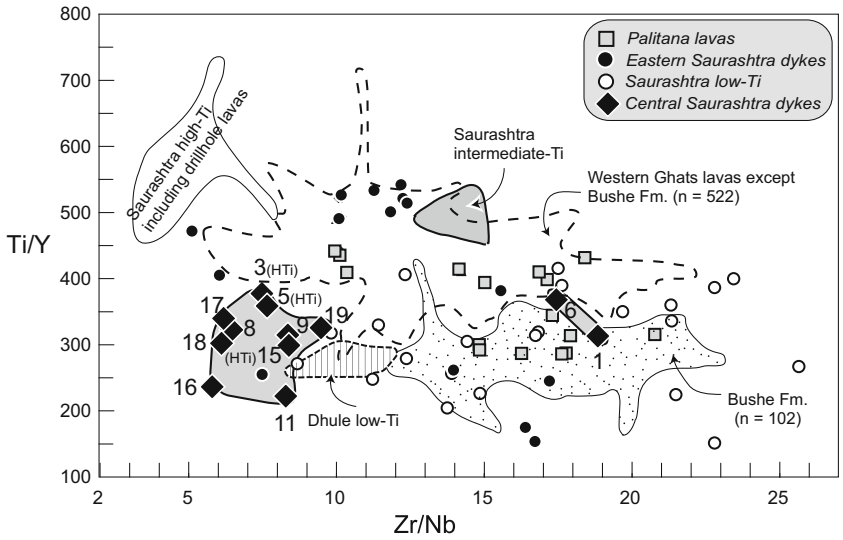

Fig. 9 Plot of Ti/Y vs. Zr/Nb for various Deccan mafic lavas and dykes as well as the Central Saurashtra dykes. Data sources are as follows: the Western Ghats sequence including the Bushe Formation (total 624 samples): Beane (1988); Saurashtra high-Ti, intermediate-Ti, and low-Ti lavas: Krishnamurthy and Cox (1977), Melluso et al. (1995, 2006), and Peng and Mahoney (1995); Dhule area low-Ti flows: Melluso et al. (2004); Palitana lavas and the Eastern Saurashtra dykes: Sheth et al. (2013). Sample numbers are marked next to the Central Saurashtra dyke samples and the high-Ti dykes are indicated

and CSD6 are thus significantly contaminated by upper continental crust, an inference supported by their Sr–Nd isotopic ratios. The scenario is similar to that observed by Sheth et al. (2013) for the Eastern Saurashtra dyke swarm, in which four dykes are highly crustally contaminated, but the majority much less so.

We performed modeling of combined assimilation and fractional crystallization (AFC, DePaolo 1981) to reproduce the trace element and isotopic variations in the Central Saurashtra dykes. The nature of the Precambrian crustal basement beneath Saurashtra is unknown because of lack of outcrops or xenoliths, but the Western Dharwar Craton, exposed south of the Deccan Traps, may extend to at least the central Deccan Traps (the Dhule area, Fig. 1a, Ray et al. 2008). We therefore took a granite from the Western Dharwar Craton (Jayananda et al. 2006) as a putative contaminant and the low-Ti basalt dyke CSD16 (initial $^{143}Nd/^{144}Nd=0.512621$; $\varepsilon_{Nd}t = +1.3$) as the starting magma. Note that low-Ti basalt dyke CSD11 has the most "primitive" or mantle-like isotopic ratios (initial $^{143}Nd/^{144}Nd=0.512770$; $\varepsilon_{Nd}t=+4.2$) of all dykes, but its $^{40}Ar/^{39}Ar$ age of 62.4 Ma shows that it was emplaced several million years after the bulk of the swarm and is therefore unsuitable as the magma end member in the AFC modeling.

The results of the AFC modeling are shown in Fig. 10a, b. The AFC curve indicates that the most contaminated sample (low-Ti basaltic andesite CSD6) could be derived by ~40 % fractional crystallization coupled with ~12 % assimilation of the granite. AFC modeling using a low-Ti starting magma fails to reproduce the geochemical variations observed in the high-Ti rocks CSD3, 5, 15 and requires unrealistically high degrees of fractionation (~80 %) with extreme iron enrichment. This further suggests that the low-Ti and high-Ti Central Saurashtra dyke rocks originated from distinct parental magmas.

Lateral geochemical variations in dykes, and their significance

Lateral geochemical variations (both elemental and isotopic) in individual Deccan dykes have been discussed by Bondre et al. (2006), Ray et al. (2007), Vanderkluysen et al. (2011), and Sheth et al. (2013), and our data provide some additional insights on this issue. As seen in Fig. 1c, the Central Saurashtra dyke swarm includes several long dykes, which we sampled at various locations in order to determine their lateral petrographic and geochemical variations. This can provide useful information about magma transport in the dyke including the magma flow direction. In the field, inadequate exposure often prevents continuous lateral tracing of dykes. Thus, the Sardhar dyke, the longest in Saurashtra (Auden 1949) forms a continuous topographic ridge over ~40 km from the west of Ribda (sample CSD1) to the east of Sardhar (sample CSD5), but its further eastward extension is less certain. It would appear from Fig. 1c that the dyke extends to the east of Kundani (sample CSD3). If so, it is slightly arcuate in trace and at least 62 km in length. As noted above, 62 % fractional crystallization of the Sardhar basalt CSD1 (with the extract containing olivine:plagioclase:clinopyroxene in 22:42:36 ratio) can reproduce the Sardhar basaltic andesite CSD5 located 23 km to the east. This scenario is however untenable if we consider the Nd–Sr isotopic ratios of CSD1 ($\varepsilon_{Nd}t=-8.2$, initial $^{87}Sr/^{86}Sr=0.714212$) and CSD5 ($\varepsilon_{Nd}t=-3.7$, initial $^{87}Sr/^{86}Sr=0.707547$), indicating that the latter is much less contaminated. A

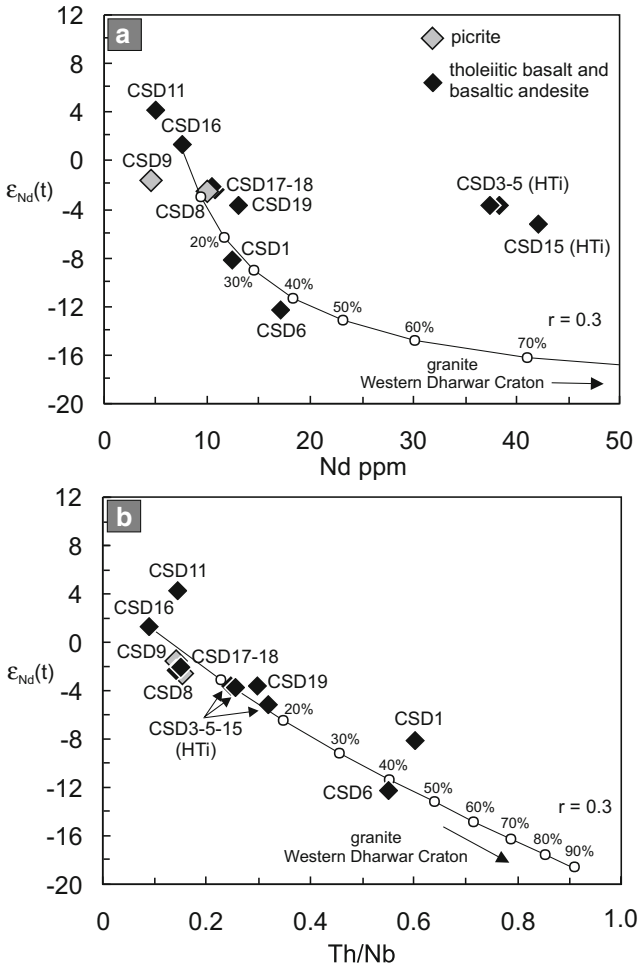

Fig. 10 **a** and **b** Assimilation-fractional crystallization (AFC; DePaolo 1981) model for the Central Saurashtra dykes. r = $mass_{assimilated}$/$mass_{cumulated}$; f = residual liquid fraction. Bulk distribution coefficients (D) have been estimated using the proportions of minerals in the fractional crystallization extracts (obtained from mass balance calculations) in combination with mineral–liquid distribution coefficients for olivine, clinopyroxene, and plagioclase from the literature (GERM website; http://www.earthref.org). Assumed bulk partition coefficients are: D_{Nd}=0.2; D_{Nb}=0.01; D_{Th}=0.01. The numbers close to the AFC curves indicate the residual liquid fraction (f). Crustal contaminant values used in the AFC models are from Jayananda et al. (2006) (sample IND412; Nd=28.2 ppm, Nb=15.8 ppm, Th=34.8 ppm; present day $^{143}Nd/^{144}Nd$=0.511082, ε_{Nd}=−30.4; $^{143}Nd/^{144}Ndt$=0.511032, $\varepsilon_{Nd}t$=−29.7 corrected for an age of 65 Ma). Starting composition for the Central Saurashtra dykes is the sample CSD16 (Nd=7.6 ppm, Nb=9.7 ppm, Th=0.86 ppm, $^{143}Nd/^{144}Nd$=0.512621 at 65 Ma, $\varepsilon_{Nd}t$=+1.3)

possible explanation is that, as seen in outcrop, the Sardhar dyke is made up of multiple magma injections (see Fig. 8c of Sheth and Cañón-Tapia 2015), and samples CSD1 and CSD5 do not belong to a single magma batch.

Interestingly, whereas the Sardhar dyke sample CSD1 is low Ti, sample CSD5 (taken at Sardhar village) is high Ti, and sample CSD3 (taken 20 km east of Sardhar near Kundani) is also high Ti. At Kundani (Fig. 1c), where CSD3 was sampled, only one dyke zone is exposed (see Fig. 5d of Sheth and Cañón-Tapia 2015). Nd–Sr isotopic ratios of CSD3 ($\varepsilon_{Nd}t$=−3.6, $^{87}Sr/^{86}Sr$=0.707521) are identical within analytical error to those of sample CSD5. This provides some valuable insights: (i) sample CSD3 represents the eastward lateral extension of the Sardhar dyke, which is thus at least 62 km long, from the west of Ribda to the east of Kundani (Fig. 1c), (ii) samples CSD5 and CSD3 represent the same magma batch which flowed laterally in the dyke fissure over at least 20 km without wall-rock assimilation, and (iii) the dyke was formed by several magma injections of distinct compositions, but does not expose (probably, never developed) all the constituent zones along its whole length.

Other samples collected in this study may also represent different exposed segments of the same individual dykes. Two such pairs are CSD13–CSD15 and CSD16–CSD14 (Fig. 1c), but we did not analyze CSD13 and CSD14 for isotopic ratios and therefore cannot fully evaluate how homogeneous these dykes are laterally. However, as for the Sardhar dyke, we sampled the long (30 km) and prominently curved Isapur-Charkha dyke (Fig. 1c), at three locations (samples CSD8, CSD7 and CSD18 taken progressively eastwards). We do not have isotopic data for the middle sample (CSD7), but the isotopic data for picrite CSD8 ($\varepsilon_{Nd}t$=−2.6, $^{87}Sr/^{86}Sr$=0.707096) and basalt CSD18 ($\varepsilon_{Nd}t$=−2.1, $^{87}Sr/^{86}Sr$=0.707068) are identical within error. This is consistent with the two samples representing a single, isotopically homogeneous dyke with a prominently curved trace and a minimum length of 30 km, in which magma flowed eastward over ≥30 km fractionating olivine, but without wall-rock assimilation.

Stratigraphic implications of dyke geochemistry: dyke-flow correlations

As noted, the Central Saurashtra dykes cut Deccan basalt lava flows at the present level of exposure. One of the aims of this study was to determine whether these dykes fed lava flows at higher levels, whose erosional remnants are potentially represented in the variably Ti-enriched Saurashtra flows sampled by Melluso et al. (1995), the high-Ti drillhole sequences of NE Saurashtra (West 1958; Krishnamurthy and Cox 1977; Peng and Mahoney 1995; Melluso et al. 2006), and the low-Ti-dominated Palitana flow sequence (Sheth et al. 2013). The $^{40}Ar/^{39}Ar$ ages of 65–66 Ma for the Sardhar dyke (sample CSD5) and the Isapur-Charkha dyke (sample CSD8) indicate that these dykes were emplaced at the same time as the bulk of the Deccan province in the Western Ghats (see Baksi 2014 and references therein), the high-Ti drillhole sequences (Peng and Mahoney 1995) and the alkalic plugs of Kachchh (Pande et al. 1988). The dyke CSD11 was emplaced much later, in the Palaeocene, at ~62.4 Ma, and differs significantly from all other dykes by virtue of its highest $(^{143}Nd/^{144}Nd)_t$ (0.512770) and $\varepsilon_{Nd}t$ (+4.2), and its low La/Sm (1.85) and Th/Nb (0.15), suggesting little crustal contamination. Interestingly, Deccan basalt flows around Ninama, north of Vinchhiya (just out of the map in Fig. 1c), have been inferred to

be of Palaeocene age based on palynoflora in the associated intertrappean sedimentary beds (Samant et al. 2014), and dyke CSD11 may have fed one of them. We have recently sampled these flows (H. Sheth and R. Duraiswami, December 2014) for a geochronological and geochemical study.

In regard to the geochemical correlations of the Central Saurashtra dykes to the Saurashtra lavas, the dykes are evolved in composition and dominantly low-Ti and cannot have been feeders to the NE Saurashtra high-Ti drillhole sequences (as well as the Pavagadh sequence 150 km further east) which include many picritic flows. Even the high-Ti segment of the very long Sardhar dyke (samples CSD3 and CSD5) cannot have fed the high-Ti drillhole sequences, given their distinct Ti/Y and Zr/Nb ratios (Fig. 9).

Sheth et al. (2013) found that the Eastern Saurashtra dykes studied by them could not have fed the mainly low-Ti Palitana sequence because of their clear and complete separation in Sr–Nd isotopic composition (Fig. 5). They considered that the Palitana lavas may have been fed by dykes on the Deccan "mainland" region (such as in the Nandurbar–Dediapada areas, Fig. 1a), or by the still poorly studied dykes in southern Saurashtra around Rajula, or by the Central Saurashtra dykes, all of which outcrop at relatively small distances (100–150 km) from Palitana (Fig. 1b). Our study shows that though the Central Saurashtra dykes and the Palitana sequence are both dominated by low-Ti tholeiitic basalts, they are completely distinct in Sr–Nd isotopic composition (Fig. 5), and thus petrogenetically unrelated. The Central Saurashtra dykes are thus ruled out as possible feeders to the NE Saurashtra drillhole sequences, as well as the Pavagadh and Palitana sequences.

We also explore whether the Central Saurashtra dykes were the feeders of any of the low-Ti surface lava flows studied by Melluso et al. (1995) from a wider region in Saurashtra (Fig. 3a). The Ti/Y vs. Zr/Nb plot (Fig. 9) shows that the Central Saurashtra dykes form a very distinct cluster away from not only the Palitana lavas but also the low-Ti lavas of Melluso et al. (1995). Because these ratios do not change during fractional crystallization, Fig. 9 conclusively shows, despite the variable degrees of magmatic evolution, that the Central Saurashtra dykes are not possible feeders to any of the hitherto analyzed lava-flow successions of Saurashtra. The same conclusion was reached by Sheth et al. (2013) for the Eastern Saurashtra dykes. The feeder dykes of these lava-flow successions remain to be found.

We also consider the relationship of the Central Saurashtra dykes to the Eastern Saurashtra dykes. As seen from Fig. 5, they possess similar $^{143}Nd/^{144}Nd$ ratios, but are distinct in $^{87}Sr/^{86}Sr$ ratios, and therefore must represent genetically unrelated suites. Both dyke swarms contain a few members (Eastern Saurashtra dykes ESD3 and ESD5 analyzed for Sr–Nd isotopic ratios, and dykes ESD2 and ESD7 not analyzed for isotopic ratios, and Central Saurashtra dykes CSD1 and CSD6) which are contaminated by continental crust to much greater degrees than the majority of the dykes, but the mixing-contamination arrays in Fig. 5 are linear and tight, indicating that any alteration processes did not significantly affect the isotopic compositions. Our geochemical data on the Central Saurashtra dykes, combined with those of Sheth et al. (2013) on the Palitana lava flows and Eastern Saurashtra dykes, as well as those of Melluso et al. (1995) on lava flows from a wider region in Saurashtra, show that low-Ti tholeiites dominate in this region.

Melluso et al. (1995) noted that high-Ti lavas only outcrop north–northeast of a line connecting Rajkot to Palitana (Fig. 1b). This observation was strengthened by the study of Sheth et al. (2013) which included not only lava flows (potentially far travelled from their source areas) but also dykes. Intriguingly, the same observation is further supported by our new results on Central Saurashtra dykes: a line joining Rajkot to Palitana cities would go right through the Sardhar dyke (Fig. 1b), and whereas the sample CSD1 collected to the west of the line is low Ti, samples CSD5 and CSD3 to the east of the line are high Ti. The interpretation of this observation is not clear at present, but if the high-Ti basalts were derived from clinopyroxene-rich, ocean island-type mantle as discussed by Melluso et al. (1995, 2006), such mantle apparently existed under Saurashtra only east of the Rajkot–Palitana line and under the adjacent Cambay rift ca. 65 Ma ago.

Conclusions

The Central Saurashtra mafic dyke swarm in the northwestern Deccan Traps contains many subalkalic basalts and basaltic andesites along with several picrites and one andesite. We have obtained $^{40}Ar/^{39}Ar$ ages of 66–65 Ma for two of the dykes and of 62.4 Ma for a third, indicating that the swarm was formed over several million years. Mineral chemical, and whole-rock major and trace element, and Sr–Nd isotopic data for the dykes show that fractional crystallization, crystal accumulation, and crustal contamination were widespread, though the degree of contamination was small for most dykes. Crustal contamination was significant in two dykes (CSD1 and CSD6), and negligible or absent in the late-formed (62.4 Ma) basalt dyke CSD11. Most dykes can be considered low-Ti and a few are high-Ti, and these Ti variations cannot be explained by fractional crystallization processes, requiring distinct parental magmas, as argued for several other flood basalt provinces (e.g., Peate 1997; Shellnutt et al. 2014). The geochemical data provide evidence for long-distance (≥30 km) compositional homogeneity in some of the dykes, and lateral heterogeneity in some other dykes, partly because these dykes were formed by multiple magma injections which are not exposed everywhere along strike. The combined field and geochemical data establish the Sardhar multiple-injection

dyke as at least 62 km long and the longest in all of Saurashtra, and samples collected 20 km apart along this dyke have identical Sr–Nd compositions, indicating magma transport over at least that distance. However, this dyke cannot have fed the high-Ti lava sequences previously studied from Saurashtra, as shown by its distinct Ti/Y and Zr/Nb ratios, for example. The low-Ti Central Saurashtra dykes were also not feeders to the hitherto studied low-Ti lava-flow successions dominant in the Saurashtra region, because of their very distinct Sr–Nd isotopic compositions. The feeder dykes of these sequences remain to be identified. Our results support the observations of Melluso et al. (1995) and Sheth et al. (2013) that high-Ti basalt lavas and dykes in Saurashtra are found only north–northeast of a line joining Rajkot to Palitana, which therefore suggests the presence of enriched mantle under northeastern Saurashtra and under the adjacent Cambay rift at ~65 Ma.

Acknowledgments Field work was supported by the Industrial Research and Consultancy Centre (IIT Bombay) grant 09YIA001 to Sheth. Funds for EPMA analyses by Cucciniello were provided by Italian MIUR (PRIN grants 2008 to Leone Melluso). Leone Melluso is thanked for providing many unpublished Deccan Traps mineral analyses. Demonterova acknowledges the Russian Foundation for Basic Research (Grant No. 15-05-05130). ICPMS trace element and Sr–Nd isotope ratio measurements by Demonterova were performed under the framework of the Baikal Analytical Center, Irkutsk, Russia. Pande acknowledges Grant No. IR/S4/ESF-04/2003 from the Department of Science and Technology (Govt. of India) toward the development of the IIT Bombay-DST National Facility for ^{40}Ar–^{39}Ar Geo-thermochronology. Vijayan was supported by a Ph.D. fellowship from the Council of Scientific and Industrial Research (CSIR), Govt. of India. Vijayan thanks Trupti Gurav for assistance with the laboratory work at IIT Bombay. We thank Ajoy Baksi for helpful comments on an earlier version of this work. The present manuscript was much improved by the detailed, critical reviews of Zhan Peng, Greg Shellnutt, an anonymous reviewer, and Associate Editor David Peate.

References

Auden JB (1949) Dykes in western India—a discussion of their relationships with the Deccan Traps. Trans Nat Acad Sci Ind 3:123–157

Baksi AK (2014) The Deccan Trap—Cretaceous–Palaeogene boundary connection: new ^{40}Ar/^{39}Ar ages and critical assessment of existing argon data pertinent to this hypothesis. In: Sheth HC, Vanderkluysen L (eds) Flood basalts of Asia. J Asian Earth Sci 84:9–23

Beane JE (1988) Flow stratigraphy, chemical variation and petrogenesis of Deccan flood basalts from the Western Ghats, India. PhD Dissertation, Washington State Univ, USA

Beane JE, Hooper PR (1988) A note on the picrite basalts of the Western Ghats, Deccan Traps, India. In: Subbarao KV (ed) Deccan flood basalts. Geol Soc Ind Mem 10:117–133

Beane JE, Turner CA, Hooper PR, Subbarao KV, Walsh JN (1986) Stratigraphy, composition and form of the Deccan basalts, Western Ghats, India. Bull Volcanol 48:61–83

Bondre NR, Hart WK, Sheth HC (2006) Geology and geochemistry of the Sangamner mafic dyke swarm, western Deccan volcanic province, India: implications for regional stratigraphy. J Geol 114:155–170

Chatterjee N, Sheth H (2015) Origin of the Powai ankaramite, and the composition, *P–T* conditions of equilibration and evolution of the primary magmas of the Deccan tholeiites. Contrib Mineral Petrol 169:32. doi:10.1007/s00410-015-112-8

Cucciniello C, Choudhary AK, Zanetti A, Sheth HC, Vichare S, Pereira R (2014) Mineralogy, geochemistry and petrogenesis of the Khopoli mafic intrusion, Deccan Traps, India. Mineral Petrol 108:333–351

Deer WA, Howie RA, Zussman J (2001) Rock-forming minerals, vol 4A, 2nd edn. Framework silicates: feldspars. Geological Society of London, 972 pp

DePaolo DJ (1981) Trace element and isotopic effects of combined wall rock assimilation and fractional crystallization. Earth Planet Sci Lett 53:189–202

Hergt JM, Peate DW, Hawkesworth CJ (1991) The petrogenesis of Mesozoic Gondwana low-Ti flood basalts. Earth Planet Sci Lett 105:134–148

Ishii T (1975) The relations between temperature and composition of pigeonite in some lavas and their application to geothermometry. Miner J 8:48–57

Ivanov AV, Demonterova EI, Rasskazov SV, Yasnygina TA (2008) Low-Ti melts from the southeastern Siberian Traps large igneous province: evidence for a water-rich mantle source? J Earth Syst Sci 117: 1–21

Jayananda M, Chardon D, Peucat JJ, Capdevila R (2006) 2.61 Ga potassic granites and crustal reworking in the western Dharwar craton, south India: tectonic, geochronologic and geochemical constraints. Precamb Res 150:1–26

Krishnamurthy P, Cox KG (1977) Picrite basalts and related lavas from the Deccan Traps of western India. Contrib Mineral Petrol 62:53–75

Krishnamurthy P, Gopalan K, Macdougall JD (2000) Olivine compositions in picrite basalts and the Deccan volcanic cycle. J Petrol 41: 1057–1069

Krishnamurthy P, Mahoney JJ, Gopalan K, MacDougall JD (2014) Clinopyroxene compositions in the Deccan and Rajmahal Traps and their bearing on magma types and evolution. In: Sheth HC, Vanderkluysen L (eds) Flood basalts of Asia. J Asian Earth Sci 84: 102–117

Kshirsagar PV, Sheth HC, Seaman SJ, Shaikh B, Mohite P, Gurav T, Chandrasekharam D (2012) Spherulites and thundereggs from pitchstones of the Deccan Traps: geology, petrochemistry, and emplacement environments. Bull Volcanol 74:559–577

Le Bas MJ, Le Maitre RW, Streckeisen A, Zanettin B (1986) A chemical classification of volcanic rocks based on the total alkali–silica diagram. J Petrol 27:745–750

Lepage LD (2003) ILMAT: an Excel worksheet for ilmenite–magnetite geothermometry and geobarometry. Comp Geosci 29:673–678

Lindsley DH (1983) Pyroxene thermometry. Am Mineralogist 68:477–493

Ludwig KR (2012) Isoplot/Ex, v. 3.75. Berkeley Geochronology Center Special Publication No. 5, Berkeley

Lyubetskaya T, Korenaga J (2007) Chemical composition of Earth's primitive mantle and its variance: 1 Method and results. J Geophys Res 112, B03211. doi:10.1029/2005JB004223

Melluso L, Sethna SF (2011) Mineral compositions in the Deccan igneous rocks of India: an overview. In: Ray J, Sen G, Ghosh B (eds) Topics in igneous petrology. Springer, Heidelberg, pp 135–160

Melluso L, Beccaluva L, Brotzu P, Gregnanin A, Gupta AK, Morbidelli L, Traversa G (1995) Constraints on the mantle sources of the Deccan Traps from the petrology and geochemistry of the basalts of Gujarat State (western India). J Petrol 36:1393–1432

Melluso L, Barbieri M, Beccaluva L (2004) Chemical evolution, petrogenesis, and regional chemical correlations of the flood basalt sequence in the central Deccan Traps, India. In: Sheth HC, Pande K (eds) Magmatism in India through time. Proc Ind Acad Sci (Earth Planet Sci) 113:587–603

Melluso L, Mahoney JJ, Dallai L (2006) Mantle sources and crustal input as recorded in high-Mg Deccan Traps basalts of Gujarat (India). Lithos 89:259–274

Middlemost EAK (1989) Iron oxidation ratios, norms and the classification of volcanic rocks. Chem Geol 77:19–26

Morimoto N, Fabrie SJ, Ferguson AK, Ginzburg IV, Ross M, Seifert FA, Zussman J, Aoki K, Gottardi G (1988) Nomenclature of pyroxenes. Am Mineral 73:1123–1133

Panteeva SV, Gladkochoub DP, Donskaya TV, Markova VV, Sandimirova GP (2003) Determination of 24 trace elements in felsic rocks by inductively coupled plasma mass spectrometry after lithium metaborate fusion. Spectrochem Acta B58:341–350

Peate DW (1997) The Paraná-Etendeka province. In: Mahoney JJ, Coffin MF (eds) Large igneous provinces: continental, oceanic, and planetary flood volcanism. Am Geophys Union Geophys. Monogr 100: 217–245

Peng ZX, Mahoney JJ (1995) Drillhole lavas from the northwestern Deccan Traps, and the evolution of Réunion hotspot mantle. Earth Planet Sci Lett 134:169–185

Peng ZX, Mahoney J, Hooper P, Harris C, Beane J (1994) A role for lower continental crust in flood basalt genesis? Isotopic and incompatible element study of the lower six formations of the western Deccan Traps. Geochim Cosmochim Acta 58:267–288

Peng ZX, Mahoney JJ, Hooper PR, Macdougall JD, Krishnamurthy P (1998) Basalts of the northeastern Deccan Traps, India: isotopic and elemental geochemistry and relation to southwestern Deccan stratigrapy. J Geophys Res 103(B12):29843–29865

Peng ZX, Mahoney JJ, Hooper PR, Vanderkluysen L (2014) Nd, Sr and Pb isotopic and chemical compositions of central Deccan Traps lavas and their relation to southwestern Deccan stratigraphy. In: Sheth HC, Vanderkluysen L (eds) Flood basalts of Asia. J Asian Earth Sci 84:83–94

Pin C, Santos-Zalduegui JF (1997) Sequential separation of light rare-earth elements, thorium and uranium by miniaturized extraction chromatography: application to isotopic analyses of silicate rocks. Anal Chim Acta 339:79–89

Pin C, Briot D, Bassin C, Poitrasson F (1994) Concomitant separation of strontium and samarium–neodymium for isotopic analysis in silicate samples, based on specific extraction chromatography. Anal Chim Acta 298:209–217

Putirka K (2008) Thermometers and barometers for volcanic systems. In: Putirka K, Tepley F (eds) Minerals, inclusions and volcanic processes, vol 69, Rev Mineral Geochem, vol. American Mineralogical Society, Washington, DC, pp 61–120

Rasskazov SV, Saranina EV, Demonterova EI, Maslovskaya MN, Ivanov AV (2002) Mantle components in Late Cenozoic volcanics of the East Sayan (from Pb, Sr, and Nd isotopes). Geol Geofiz 42:1065–1079

Ray R, Sheth HC, Mallik J (2007) Structure and emplacement of the Nandurbar–Dhule mafic dyke swarm, Deccan Traps, and the tectonomagmatic evolution of flood basalts. Bull Volcanol 69: 531–537

Ray R, Shukla AD, Sheth HC, Ray JS, Duraiswami RA, Vanderkluysen L, Rautela CS, Mallik J (2008) Highly heterogeneous Precambrian basemenet under the central Deccan Traps, India: direct evidence from xenoliths in dykes. Gondwana Res 13:375–385

Renne PR, Swisher CC, Deino AL, Karner DB, Owens TL, DePaolo DJ (1998) Intercalibration of standards, absolute ages and uncertainties in $^{40}Ar/^{39}Ar$ dating. Chem Geol 145:117–152

Roeder PL, Emslie RF (1970) Olivine-liquid equilibrium. Contrib Mineral Petrol 29:275–289

Rudnick RL, Gao S (2003) Composition of the continental crust. In: Rudnick RL (ed) Treatise on geochemistry 3. Elsevier, pp 1–64

Samant B, Mohabey DM, Srivastava P, Thakre D (2014) Palynology and clay mineralogy of the Deccan volcanic associated sediments of Saurashtra, Gujarat: age and palaeoenvironments. J Earth Syst Sci 123:219–232

Sen A, Pande H, Hegner E, Sharma KK, Dayal AM, Sheth HC, Mistry H (2012) Deccan volcanism in Rajasthan: $^{40}Ar–^{39}Ar$ geochronology and geochemistry of the Tavidar volcanic suite. J Asian Earth Sci 59: 127–140

Shellnutt JG, Bhat GM, Wang K-L, Brookfield ME, Jahn B-M, Dostal J (2014) Petrogenesis of the flood basalts from the Early Permian Panjal Traps, Kashmir, India: geochemical evidence for shallow melting of the mantle. Lithos 204:159–171

Sheth HC, Cañón-Tapia E (2015) Are flood basalt eruptions monogenetic or polygenetic? Int J Earth Sci. doi:10.1007/s00531-014-1048-z

Sheth HC, Melluso L (2008) The Mount Pavagadh volcanic suite, Deccan Traps: geochemical stratigraphy and magmatic evolution. J Asian Earth Sci 32:5–21

Sheth HC, Ray JS, Ray R, Vanderkluysen L, Mahoney JJ, Kumar A, Shukla AD, Das P, Adhikari S, Jana B (2009) Geology and geochemistry of Pachmarhi dykes and sills, Satpura Gondwana Basin, central India: problems of dyke-sill-flow correlations in the Deccan Traps. Contrib Mineral Petrol 158:357–380

Sheth HC, Choudhary AK, Bhattacharyya S, Cucciniello C, Laishram R, Gurav T (2011) The Chogat-Chamardi subvolcanic complex, Saurashtra, northwestern Deccan Traps: geology, petrochemistry, and petrogenetic evolution. J Asian Earth Sci 41:307–324

Sheth HC, Choudhary AK, Cucciniello C, Bhattacharyya S, Laishram R, Gurav T (2012) Geology, petrochemistry, and genesis of the bimodal lavas of Osham Hill, Saurashtra, northwestern Deccan Traps. J Asian Earth Sci 43:176–192

Sheth HC, Zellmer GF, Kshirsagar PV, Cucciniello C (2013) Geochemistry of the Palitana flood basalt sequence and the Eastern Saurashtra dykes, Deccan Traps: clues to petrogenesis, dyke-flow relationships, and regional lava stratigraphy. Bull Volcanol 75:701. doi:10.1007/s00445-013-0701-x

Sheth HC, Zellmer GF, Demonterova EI, Ivanov AV, Kumar R, Patel RK (2014) The Deccan tholeiite lavas and dykes of Ghatkopar-Powai area, Mumbai, Panvel flexure zone: geochemistry, stratigraphic status,and tectonic significance. In: Sheth HC, Vanderkluysen L (eds) Flood basalts of Asia. J Asian Earth Sci 84:69–82

Stormer JC, Nicholls J (1978) XLFRAC: a program for interactive testing of magmatic differentiation models. Comp Geosci 4:143–159

Sun S-s, McDonough WF (1989) Chemical and isotopic systematics of oceanic basalts: implications for mantle composition and processes. In: Saunders AD, Norry MJ (eds) Magmatism in the ocean basins. Geol Soc Spec Pub 42:313–345

Vanderkluysen L, Mahoney JJ, Hooper PR, Sheth HC, Ray R (2011) The feeder system of the Deccan Traps (India): insights from dyke geochemistry. J Petrol 52:315–343

Verma SP, Torres-Alvarado IS, Sotelo-Rodriguez ZT (2002) SINCLAS: standard igneous norm and volcanic rock classification system. Comput Geosci 28:711–715

West WD (1958) The petrography and petrogenesis of forty eight flows of Deccan Trap penetrated by borings in western India. Trans Nat Inst Sci Ind 4:1–56

Wilson SA (1997) Data compilation for USGS reference material BCR-2, Columbia River Basalt. US Geological Survey Open File Rep

Wilson SA (2000) Data compilation for USGS reference material BHVO-2, Hawaiian Basalt. US Geol Surv Open File Rep